# FRIPON: a worldwide network to track incoming meteoroids

F. Colas[1,42], B. Zanda[2,1,42], S. Bouley[3,1,42], S. Jeanne[1,42], A. Malgoyre[53,28,42], M. Birlan[1,37,18], C. Blanpain[53,28], J. Gattacceca[5,16,28], L. Jorda[4,28], J. Lecubin[53,28], C. Marmo[3], J.L. Rault[1,7,42], J. Vaubaillon[1,42], P. Vernazza[4,28], C. Yohia[53,28] A. Steinhausser[2,42], P. Abraham[54,13], S. Anghel[157,37,74], E. Antaluca[55,25], K. Antier[7,42,44], T. Appere[56,13], Y. Audureau[3], G. Auxepaules[57,14], R. Baldo[58,21], D. Baratoux[59,22], E. Barbotin[60,27], M. Bardy[61,17], D. Barghini[52,30,36], O. Bautista[62,10], L. D. Bayle[63,11], P. Beck[64,65,29], R. Behrend[66,41], M. Benammi[67,27], E. Beneteau[68,26], Z. Benkhaldoun[38,69], F. Bergamini[70,15], F. Bettonvil[50,35], D. Bihel[71,24], C. Birnbaum[42,43], O. Blagoi[157,37], I. Boaca[157,37], B. Bobiet[72,13], E. Bouchet[196,41], E. Bouchez[73,29], D. Boust[75,24], V. Boudon[76,12], T. Bouman[77,9], P. Bourget[78,31], S. Brandenburg[49,35], Ph. Bramond[79,22], E. Braun[80,22], P. Cacault[81,11], B. Caillier[82,22], A. Calegaro[137,33], J. Camargo[83,39], S. Caminade[8], A.P.C. Campana[84,16], P. Campbell-Burns[190,45], O. Carell[71,24], S. Carreau[85,27], P. Cavier[86,14], S. Celestin[87,14], A. Cellino[30,36], M. Champenois[89,21], H. Chennaoui[92,69], P. Cholvy[139,28], L. Chomier[90,29], A. Christou[91,45], P. Coadou[103,22], F. Cochard[93,29], S. Cointin[94,28], J.Y. Cocaign[95,24], L. Corp[96,22], F. Costard[3,24], M. Cottier[196,41], P. Cournoyer[187,188], E. Coustal[98,19], J.C. Cuzon[72,13], C. Danescu[157,186,37], A. Dardon[99,11], C. Davadan[100,10], V. Debs[101,9], J. P. Defaix[202,12], P. Defives[103,22], F. Deleflie[1,23], P. De Luca[104,14], A. Dias[53,28], M. Dimartino[30,36], F.M. Dominici[16], E. Drolshagen[158,40], G. Drolshagen[158,40], A. Drouard[4,28], J. L. Dumont[104,14], P. Dupouy[105,10], L. Duvignac[106,14], A. Egal[107,197,1], N. Esseiva[108,17], A. Ebel[109,15], B. Eisengarten[40,201], G. Ferrant[110,16], E. Ferreol[111,29], L. Ferriere[32,114], P. Finitzer[101,9], M. Forcier[187,188], A. Foucault[80,22], P. Francois[115,25], M. Frîncu[184,185,37], J.L. Froger[81,11], F. Gaborit[116,28], J. Galard[117,26], D. Gardiol[30,36], M. Garmier[118,18], M. Garnung[87,14], B. Gautier[119,29], D. Gerard[109,15], A. Grandchamps[187,188], B. Grouiez[120,15], S. Groult[122,23], E. Huet[123,126], Y. Hello[125,126], X. Henry[28,127], G. Herbreteau[128,19], O. Hernandez[187,188], M. Herpin[129,10], P. Hewins[1,42], J. Horak[193,45], R. Hueso[198,199,34], F. Hyaume[130,14], J.J. Hillairet[131,27], Y. Isselin[70,15], P. Janeux[133,12], P. Jeanneret[132,24], E. Jehin[134,33], M. Jobin[187,188], K. Jobse[48,35], S. Jouin[24,44], J.M. Jouvard[135,12], K. Joy[189,45], J.F. Julien[18], R. Kacerek[190,45], M. Kempf[136,40], A. King[191,45], D. Koschny[35,40,46,200], C. Krier[72,13], M.K. Kwon[1], D. Lachat[159,41], H. Lamy[137,33], J. Laskar[1,18], M. Leblanc[138,24], J.P. Lebreton[87,14], P. Le Du[112,13], F. Lelong[113,24], J.F. Leoni[139,28], A. Le-Pichon[140,24], P. Le-Poupon[130,14], A. Leroy[141,18], A. Levansuu[142,28], E. Lewin[64,65,29], A. Lienard[94,28], S. Loehle[143,40], D. Loizeau[165,29], L. Luciani[144,16], M. Maignan[130,14], S. Mancuso[30,36], E. Mandon[132,24], N. Mangold[145,26], L. Maquet[1,23], D. Marant[146,23], Y. Marchal[77,9], J.L. Marin[28], J.C. Martin-Brisset[147,14], D. Martin[192,45], D. Mathieu[148,21], F. Meyer[149,17], J. Y. Meyer[110,29], E. Meza[88], J.J. Moiroud[194,195], M. Millan[197,34], S. poppe[40,150], B. Monflier[151,22], A. Monkos[40,202], R. Moreau[152,12], J. Morin[153,19], R. Mourgues[154,26], O. Mousis[4,28], C. Nablanc[155,20], A. Nedelcu[157,37], C. Nitschelm[156,31], P. Notez[146,23], T. Ott[158,40], M. Ory[159,41], M. Pajuelo[88], G. Pallier[155,20], G. Pavy[131,27], L. Perez[113,24], S. Pérez-Hoyos[198,199,34], N. Parisot[160,20], V. Perlerin[7,42,44], A. Peyrot[124,126], F. Peth[121,15], V. Pic[161,19], C. Pilger[40,204], M. Piquel[162,13], B. Poppe[158,40], M. Poppe[205], L. Portois[163,25], J. Prezeau[164,11], C. Quantin[165,29], G. Quitte[166,22], S. Rasetti[30,36], E. Ravier[90,29], S.J. Ribas[167,168,34], D. Richard[169,10], J.P. Rivet[170,28], S. Rochain[98,19], J.F. Rojas[198,199,34], M. Rotaru[2,42,43], M. Rotger-Languereau[120,15], P. Rougier[171,20], P. Rousselot[149,17], J. Rousset[139,28], D. Rousseu[129,10], J. Rowe[45], O. Rubiera[197,34], R. Rudawska[35,51], J. Rudelle[172,10], J.P. Ruguet[169,10], S. Sales[173,19], A. Sanchez-Lavega[198,199,34], O. Sauzereau[174,26], M. Schieffer[175,17], D. Schreiner[176,23], Y. Scribano[153,19], L. Shengold[89,21], A. Shuttleworth[190,45], S. Sohy[134,33], A. Smedley[189,45], M. Tagger[87,14], P. Tanga[170,28], J.P. Teng[124,126], O. Thizy[93,29], A. Toni[46,35], R. Trangosi[141,18], B. Tregon[177,10], A. Tukkers[47,35], M. Valenzuela[178,31], G. Varennes[19], J. Vergne[179,9], M. Verlinden[180,23], M. Vidal-Alaiz[16], R. Vieira-Martins[83,39], A. Viel[18,29], V. Vinogradoff[97,28], M. Wendling[182,9], P. Wilhelm[183,9], and K. Wohlgemuth[40,203]

*(Affiliations can be found after the references)*

## ABSTRACT

*Context. ...*
*Aims. ...*
*Methods. ...*
*Results. ..*
*Conclusions. ...*

**Key words.** fireball – meteorite – interplanetary matter – Fireball network

# 1. Abstract

*Context:* Until recently, camera networks designed for monitoring fireballs worldwide were not fully automated, implying that in case of a meteorite fall, the recovery campaign was rarely immediate. This was an important limiting factor as the most fragile - hence precious - meteorites must be recovered rapidly to avoid their alteration.

*Aims:* To overcome this limitation, a fully automated camera network called FRIPON (Fireball Recovery and InterPlanetary Observation Network; PI: F. Colas) has been designed and deployed over a significant fraction of Western Europe and a small fraction of Canada. As of today, it consists of 150 cameras covering an area of about $1.5 \times 10^6 \ km^2$.

*Methods:* The FRIPON network has been monitoring meteoroid entries since 2016, allowing the characterization of their dynamical and physical properties. In addition, the level of automation of the network makes it possible to trigger a meteorite recovery campaign only a few hours after it reached the surface of the Earth.

*Results:* Nearly 4,000 meteoroids have been detected so far and characterized by FRIPON. The distribution of their orbits appears bimodal, with a cometary population and a main belt one. Sporadic meteors amount to about 55% of all meteors. A first estimate of the absolute meteoroid flux (mag < -5 ; meteoroid size ≥~1cm) amounts to 1250 /year/$10^6 \ km^2$. Such a value is compatible with previous estimates (Halliday et al. 1996). Finally, the first meteorite was recovered in Italy thanks to the extended FRIPON network.

# 2. Introduction

The study of the physical and dynamical properties of interplanetary matter (interplanetary dust particles (IDPs), meteoroids, asteroids, comets, etc...) is crucial to our understanding of the formation and evolution of the Solar System. This matter exists in many sizes, from micron-sized dust grains to several hundred kilometer-sized bodies. Whereas the largest bodies are routinely studied via Earth-based telescopic observations as well as less frequent interplanetary missions, the smallest ones (diameter ≤10m) are essentially only observed and characterized when they enter the Earth's atmosphere as their entry generates enough light (called meteor for the smaller particles and fireball for the larger ones) to be recorded by even the simplest types of cameras.

We know that ~100 tons of extraterrestrial material collide with the Earth daily, mostly as small particles less than 0.2 mm in size (Zolensky et al. (2006), Rojas et al. (2019)). At present, these small particles called IDPs are actively being collected in the stratosphere, from polar ices (Duprat et al. 2007), and within impact features on spacecraft. For such particles, the stratospheric collections provide the least contaminated and heated samples. At the other end of the spectrum, meteorites are fragments that have survived the passage through the atmosphere without internal chemical alteration and that have been recovered at the surface of the Earth. To date, all known meteorites are pieces of either small bodies (essentially asteroids and possibly comets/trans-Neptunian objects), the Moon, or Mars, with asteroidal fragments dominating the flux of material, whereas IDPs originate mostly from comets and possibly from asteroids (Bradley et al. 1996; Vernazza et al. 2015). The most detailed information on the processes, conditions, timescales and the chronology of the early history of the Solar System (e.g., Neveu & Vernazza 2019; Kruijer & Kleine 2019 and references

therein) including the nature and evolution of the particles in the pre-planetary solar nebula has so far come from the study of all these extraterrestrial materials. Recovering intact samples of such materials is therefore a critical goal of planetary studies.

However, we are not very efficient at recovering the meteorites that hit the Earth. Estimates based on previous surveys (Bland et al. 1996) and on collected falls [Meteoritical Bulletin database] indicate that, for meteorites with masses >100g, probably less than one in five hundred that fall on Earth are currently recovered. In addition, taking France as an example, recovery rates were significantly higher in the XIXth century than they are now: 45 meteorites were observed to fall and found on the ground in the XIXth century, whereas they were five times fewer in the XXth century (Fig. 1), showing that there is at present a large potential for improvement. Hot and cold deserts are privileged dense collection areas, but most meteorites are found hundreds and up to millions of years after their fall (Hutzler et al. 2016; Drouard et al. 2019). They have thus been exposed to terrestrial alteration, which has partly obliterated the scientific information they contain. Also, the information regarding their pre-atmospheric orbit is no longer available.

The most efficient approach for recovering freshly-fallen meteorites is to witness their bright atmospheric entry via dense (60-120 km spacing) camera/radio networks. These networks make it possible to accurately measure their trajectory from which both their pre-atmospheric orbit and their fall location (with an accuracy of the order of a few hundred meters) can be constrained.

Records of incoming meteorites started with the appearance of photographic plates at the end of the XIXth century, but it was only in the mid-XXth century that the first fireball observation networks were developed with the aim of recovering meteorites. Two such networks were established in the 1960s. The first one was the Prairie Network (McCrosky & Boeschenstein 1965) in the center of the United States, which remained operational from 1964 to 1975. It comprised 16 stations, 250 km apart. This network only recovered one meteorite (Lost City, 1970 - McCrosky et al. 1971). Its low efficiency despite the large area it covered (750,000 $km^2$), resulted from the distance between the stations being too large. The terminations of the fireballs (at an altitude between 30 and 20 km to yield a meteorite) were too low on the horizon and hence often perturbed by clouds and light pollution. The European Fireball Network (EFN) was also developed in the 1960s, under the guidance of the Ondrejov Observatory, following the recovery of the Píbram meteorite in 1959 (Ceplecha 1960). It is still active and has spread throughout Europe, currently covering $1 \times 10^6 \ km^2$ with about forty camera (Oberst et al. 1998). So far, it has enabled the recovery of nine meteorites (Table 1). In 1971, the MORP project (Meteorite Observation and Recovery Project - Halliday et al. 1978; Jones et al. 2005) was established over part of Canada, and led to the Innisfree recovery (Halliday et al. 1978). It comprised 16 cameras and covered a surface area of 700,000 $km^2$. Other networks using photographic techniques were also developed, such as the Tajikistan Fireball Network (Kokhirova et al. 2015), which consists of 5 cameras and covers 11,000$km^2$. However, none of these other networks has made it possible to recover meteorites so far. Last, the Desert Fireball Network (Bland et al. 2012) started in Australia in 2007. It is based on high-resolution digital cameras and made it possible to recover four meteorites.

As of today, there are 38 meteorites with reliable orbits reconstructed, 22 of which were detected by camera networks (see Table 1). Among the remaining 16 meteorites, 14 are the result of random visual observations such as the Chelyabinsk event
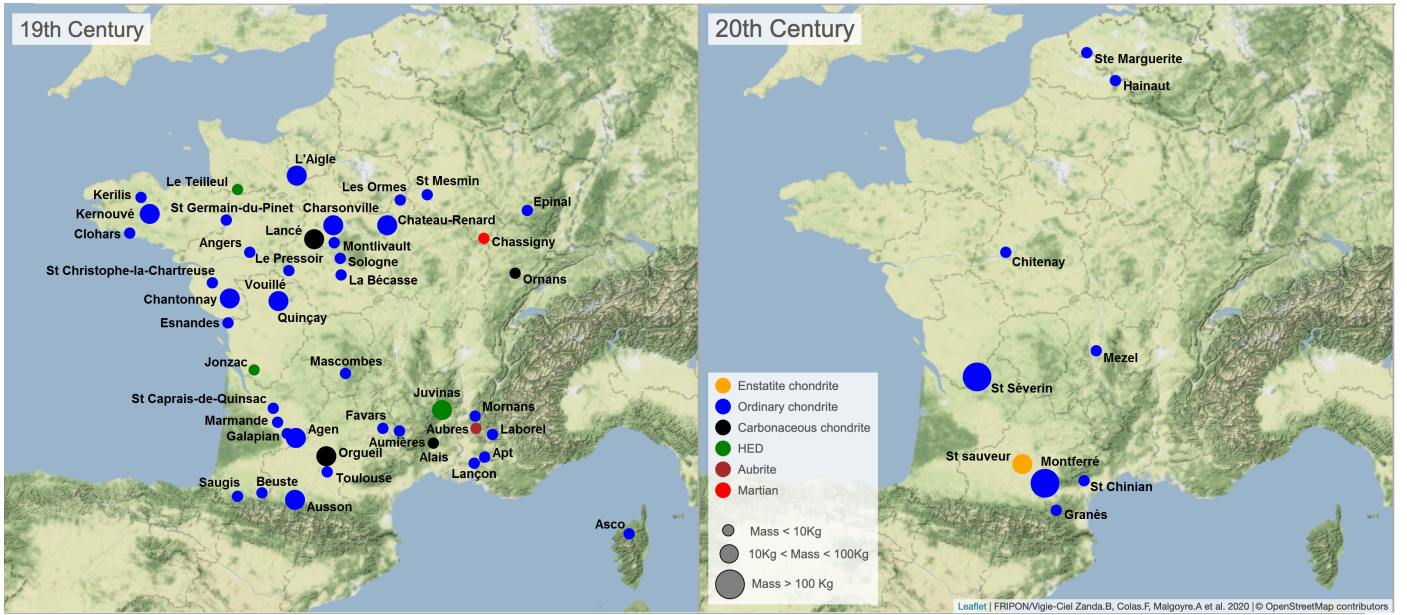
**Fig. 1.** In 19th century France, 45 meteorites were recovered after their fall was observed, a number that fell by a factor of 5 in the 20th century. Even in the 19th century, witnessed falls are not randomly distributed: they are mostly located in the great river plains (Seine and Loire in the North-West, Garonne in the South-West and Rhône valley in the South-East). In these regions, the population was denser, the view is free of obstacles (such as mountains) and the skies are often clear. The striking difference between the two centuries illustrates the need for distributed observers for meteorite recovery: rural populations declined due to urbanization in 20th century. A camera network such as FRIPON can monitor atmospheric entries and take over that role which was previously played by human observers. However, trained human eyes are still required to recover the meteorites: this is the aim of the Vigie-Ciel citizen science program (Colas et al. 2015).

(data from security cameras were used for orbit computation - Borovička et al. 2013a) and 2 meteorites were detected as asteroids before their fall (Almahata Sitta and 2018LA). During the same time interval (1959-2020), 397 meteorites were recovered after their fall was eye-witnessed (Meteoritical Bulletin Database).

The main limitation of current networks is their size. Most of them consist of a fairly small number of cameras spread over a comparatively small territory. Altogether, they cover only 2% of the surface of the Earth (Devillepoix et al. 2020). This implies that the number of bright events per year witnessed by these networks is small and that tens of years would be necessary to yield a significant number (≥100) of samples.

To overcome this limitation, a network called FRIPON (PI: F. Colas) has been designed and deployed over a large fraction of Western Europe and a small fraction of Canada (see Fig. 2). As of today, it consists of 150 cameras and 25 radios, and covers an area of $1.5 \times 10^6 \ km^2$ (section 3). The FRIPON network is coupled in France with the Vigie-Ciel citizen science program, the aim of which is to involve the general public in the search for meteorites in order to improve their recovery rate. In the present paper, we first describe the technology of the FRIPON network, its architecture, and finally the first results obtained after 4 years of observations and the first meteorite recovery in Italy[1].

## 3. The FRIPON Network

### 3.1. General description of the network

The FRIPON network was originally designed by a core team of six French scientists from the Paris Observatory (IMCCE), the French National Museum of Natural History (MNHN-IMPMC), Université Paris-Saclay (GEOPS) and Aix-Marseille University

(LAM / CEREGE / OSU Pythéas) to: i) monitor the atmospheric entry of fireballs (interplanetary matter with typical sizes greater than ~1 centimeter), ii) characterize their orbital properties to constrain both their origin and fall location, and iii) recover freshly fallen meteorites. It benefited from a grant from the French National research agency (Agence Nationale de la Recherche: ANR) in 2013 to install a network of CCD cameras and radio receivers to cover the entire French territory. Specifically, the grant was used to define the hardware (section 3.2) building on experience gained from previous networks; develop an efficient and automatic detection and data reduction pipeline (section 3.3); and build centralized network and data storage architectures (section 3.2.3). In contrast to previous networks, FRIPON is designed as a real-time network with the aim of triggering a field search within the 24h that follow the fall in order to recover fresh meteorites. As of today, FRIPON-France consists in 105 optical allsky cameras and 20 antennas for radio detection. These assets are homogeneously distributed over the territory although the radio network is slightly denser in the South of France (Fig. 2).

Starting from 2016, scientists from neighbouring countries were interested in using the hardware, the software and the infrastructure of FRIPON-France. This is the case for Italy (FRIPON-PRISMA network; Gardiol et al. 2016; Barghini et al. 2019), Germany (FRIPON-Germany), Romania (FRIPON-MOROI network; Anghel et al. 2019a; Nedelcu et al. 2018), the United Kingdom (FRIPON-SCAMP), Canada (FRIPON-DOME), the Netherlands (FRIPON-Netherlands), Spain (FRIPON-Spain), Belgium (FRIPON-Belgium), and Switzerland (FRIPON-Switzerland). Single FRIPON cameras have were also made available to several countries in order to initiate collaboration: Austria, Brazil, Chile, Denmark, Mexico, Morocco, Peru and Tunisia. As of today, 150 FRIPON cameras are operational around the world (see Fig. 2).

---

[1] Discovered from observations by the FRIPON-PRISMA network.
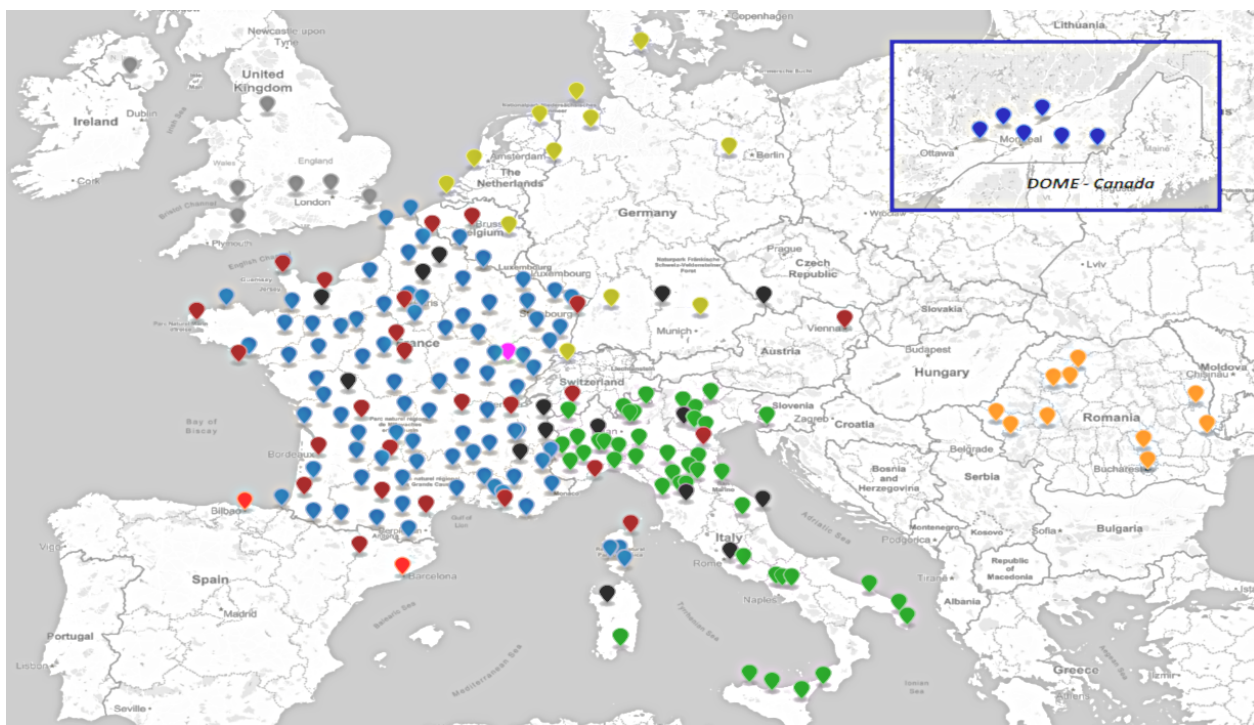
**Fig. 2.** FRIPON network map as of end 2019. The color code is the following:
1. Blue: FRIPON-Vigie-Ciel, optical stations (France), 2. Red: Coupled optical camera and radio receiver stations, 3. Black: Stations under development, 4. Green: PRISMA (Italy), 5. Light Orange: MOROI (Romania), 6. Yellow: FRIPON-North (Northern-Europe), 7. Grey: SCAMP (United Kingdom), 8. Dark blue: DOME (Canada), 9. Dark Orange: SPMN (Spain).

FRIPON is organized as a federation of the above mentioned national networks with all the cameras monitored and remotely controlled by the SIP team of the Pythéas Institute (Aix-Marseille University, France) who maintain the whole network with the support of the scientific team. All the data from the FRIPON network are stored and processed in Marseille. The data processing consists of monthly astrometric and photometric reduction of the calibration images and the daily processing of multi-detections. On request, national data can be sent to a different reduction pipeline for alternate processing and storage. Two databases host the data: raw data for one and higher level processed data such as orbits and trajectories for the other. These data are available to all Co-Is of the network at the following URL: https://fireball.fripon.org.

### 3.2. Hardware and observing strategy

#### 3.2.1. Optical cameras

Since the early 2000s, digital cameras have been used by all networks that are deployed to monitor fireballs. Two alternate technical solutions are adopted. The first one is based on a low resolution detector (e.g., Southern Ontario Meteor Network; Brown et al. 2011), while the second one relies on a high resolution detector (e.g., Desert Fireball Network; Bland et al. 2012). The measurements acquired by low resolution cameras can be accurate enough to compute orbits and strewn fields as long as the network is dense, with numerous cameras. For example, the Southern Ontario Meteor Network, which has been operating in Canada since 2004, led to the recovery of the Grimsby meteorite (Brown et al. 2011). In the case of the FRIPON network, we followed the philosophy of the Canadian Fireball Network (Brown et al. 2011) as detailed hereafter.
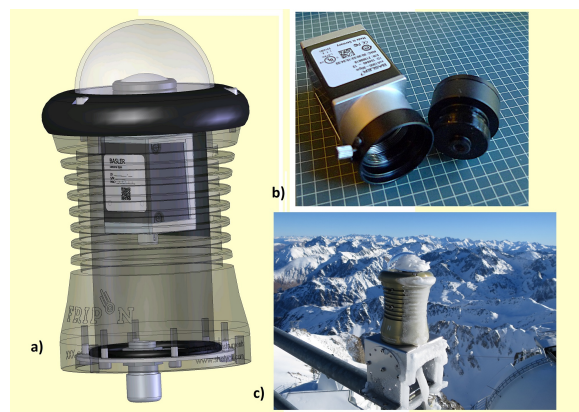


**Fig. 3.** Mosaic of "technology" developed for the FRIPON network: a) Final design of optical detectors[2]; b) Core device comprising a GigaBit Ethernet camera and fish-eye optics; c) FRIPON optical camera installed on the platform of Pic du Midi Observatory (2,876 meters altitude), in use during harsh weather conditions.

We use a CCD Sony ICX445 chip with 1296x964 pixels and a pixel size of 3.75 x 3.75 microns. For the optical design, we use a 1.25 mm focal length F/2 fish-eye camera lens, which leads to a pixel scale of 10 arcmin. Given that fireballs are typically observed from an altitude between 100 km and 40 km, we designed a network with a median distance of 80 km between cameras in order to perform an optimal triangulation. Jeanne et al. (2019) showed that the astrometric accuracy is of the order of 1 arcmin, equivalent to 30 m at a distance of 100 km. In section 4, we show that the final accuracy on the trajectory is of the order of 20 m for the position and of 100 m/s for the velocity, a value that is

**Table 1.** 38 known meteorites with reliable orbit reference discovered by networks ("N"), visual observations ("V") or telescopic observations ("T"). Bibliographic references: [1] Ceplecha 1960; [2] McCrosky et al. 1971; [3] Halliday et al. 1981; [4] Spurný et al. 2014; [5] Brown et al. 1994; [6] Brown et al. 1996; [7] Borovicka et al. 2003; [8] Brown et al. 2000; [9] Spurný et al. 2003; [10] Simon et al. 2004; [11] Trigo-Rodríguez et al. 2006; [12] Trigo-Rodríguez et al. 2009; [13] Spurný et al. 2012; [14] Chodas et al. 2010; [15] Fry et al. 2013; [16] Brown et al. 2011; [17] Spurný et al. 2010; [18] Haack et al. 2010; [19] Dyl et al. 2016; [20] Borovicka et al. 2013b; [21] Borovička et al. 2015; [22] Jenniskens et al. 2012; [23] Jenniskens et al. 2014; [24] Borovička et al. 2013a; [25] Spurný et al. 2020; [26] Trigo-Rodríguez et al. 2015; [27] Jenniskens et al. 2019; [28] Bland et al. 2016; [29] Devillepoix et al. 2018; [30] Jenniskens et al. 2020; [31] Bischoff et al. 2017; [32] Gritsevich et al. 2017; [33] Spurný et al. 2017; [34] Brown et al. 2019; [35] de la Fuente Marcos & de la Fuente Marcos 2018; [36] Bischoff et al. 2019; [37] Gardiol 2020; [38] Ott & Drolshagen 2020 .

| Year | Location | Type | Method | Ref |
|------|----------|------|--------|-----|
| 1959 | Příbram | H5 | N | [ 1] |
| 1961 | Lost City | H5 | N | [ 2] |
| 1975 | Innisfree | L5 | V | [ 3] |
| 1991 | Benešov | LL3.5 | N | [ 4] |
| 1992 | Peekskill | H6 | V | [ 5] |
| 1994 | St-Robert | H5 | V | [ 6] |
| 2000 | Morávka | H5 | N | [ 7] |
| 2000 | Tagish Lake | C2-ung | V | [ 8] |
| 2002 | Neuschwanstein | EL6 | N | [ 9] |
| 2003 | Park Forest | L5 | V | [10] |
| 2004 | Villalbeto de la Peña | L6 | N | [11] |
| 2007 | Cali | H/L4 | V | [12] |
| 2007 | Bunburra Rockhole | Eucrite | N | [13] |
| 2008 | Almahata Sitta | Ureilite | T | [14] |
| 2008 | Buzzard Coulee | H4 | V | [15] |
| 2009 | Grimsby | H5 | N | [16] |
| 2009 | Jesenice | L6 | N | [17] |
| 2009 | Maribo | CM2 | V | [18] |
| 2010 | Mason Gully | H5 | N | [19] |
| 2010 | Košice | H5 | N | [20] |
| 2011 | Križevci | H6 | N | [21] |
| 2012 | Sutter's Mill | C | V | [22] |
| 2012 | Novato | L6 | N | [23] |
| 2013 | Chelyabinsk | LL5 | V | [24] |
| 2014 | Žďár nad Sázavou | LL5 | N | [25] |
| 2014 | Annama | H5 | N | [26] |
| 2015 | Creston | L6 | N | [27] |
| 2015 | Murrili | H5 | N | [28] |
| 2016 | Dingle Dell | LL6 | N | [29] |
| 2016 | Dishchii'bikoh | LL7 | V | [30] |
| 2016 | Stubenberg | LL6 | N | [31] |
| 2016 | Osceola | L6 | V | [32] |
| 2017 | Ejby | H5/6 | N | [33] |
| 2018 | Hamburg | H4 | V | [34] |
| 2018 | 2018 LA | — | T | [35] |
| 2019 | Renchen | L5-6 | N | [36] |
| 2020 | Capodanno | — | N | [37] |
| 2020 | Novo Mesto | — | V | [38] |

required for the identification of meteorite source regions in the Solar System as shown by (Granvik & Brown 2018).

The optical device and the CCD are embedded into a special case (Fig. 3) sealed with a transparent dome allowing to record full-sky images. Moreover, these cases are equipped with a pas-sive radiator, which serves to release the heat produced by the electronics during the warm periods of the year in order to minimize CCD dark current.

Each camera is controlled by an Intel NUCi3 computer on which the data are temporarily stored. A single Power over Ethernet (PoE) cable is used for data transfer, powering and remotely managing the camera through a TPLINK (TL-SG22110P or 1500G-10PS) switch. Such a solution makes it easy to install the optical station and operate it remotely and to use cables up to 100 meters long between the camera and the computer. Fig. 3 shows the design[2] of the camera as well as its installation at Pic du Midi Observatory.

### 3.2.2. Radio receivers

In addition to optical observations, we use the powerful GRAVES radar of the French Air Force. This radar is particularly well adapted for the detection, identification and tracking of space targets including incoming meteoroids (Michal et al. 2005). Located near Dijon (central Eastern France), its four main beams transmit nominally on a half-volume located South of a line between Austria and Western France. However, the secondary radiation lobes of the radar makes it possible to also detect meteors that disintegrate in the Northern part of France. For such observations we do not need as tight a mesh as we do for optics. We have 25 stations with an average distance of 200 km, mainly in France, but also in Belgium, Italy, Switzerland, Germany, and Austria. GRAVES transmits on 143.050 MHz in a continuous wave (CW) mode 24 hours a day. A meteoroid entering the E and D layers of the Earth ionosphere produces ions and free electrons generated by the ionization of air and of meteoroid molecules. The free electrons have the property of scattering radio waves according to "back or forward meteor scatter" modes when they are illuminated by a radio transmitter.

FRIPON Radio setup (Rault et al. 2014) is a multi-static radar consisting of 25 distant receivers and an High Power Large Aperture (HPLA) radar. Thanks to its omni-directional reception antenna, each single radio station is able to receive scattered GRAVES echoes from a meteor, from its ionized trail and/or from the plasma surrounding the meteor body.

A typical FRIPON radio set-up consists of:

– a 2.5 m long vertical ground-plane antenna ref. COMET GP-5N connected to the radio receiver via a 50Ω coaxial cable model KX4;
– a general purpose Software Defined Radio (SDR) ref. FUNcube Dongle Pro + (Abbey 2013).

The ground-plane antenna radiation pattern is omni-directional in the horizontal plane, allowing both back and forward meteor scatter modes. The gain of this vertically polarized antenna is around 6 dBi. The FUNcube SDR is connected to one of the USB ports of the station and the $I/Q$ data produced by the radio are recorded 24 hours a day on the local computer hard disk. The SDR is a general coverage receiver (Fig. 4), whose main characteristics are:

– Frequency range 150 kHz to 240 MHz and 420 MHz to 1.9 GHz;
– Sensitivity: typically 12 dB SINAD NBFM for $0.15\mu V$ at 145 MHz;
– Reference oscillator stability: 1.5 ppm;
– Sampling rate: 192 kHz;

---

[2] Shelyak Instruments, www.shelyak.com

– Bit depth: 16 bits (32 bits used internally).

A Low Noise Amplifier (LNA) and a Surface Acoustic Wave (SAW) filter fitted in the front end of each receiver offer an adequate sensitivity and selectivity for the meteor echoes.
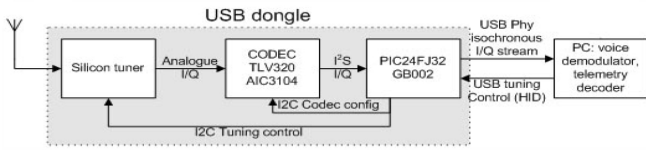


**Fig. 4.** Diagram of the FUNcube (Abbey 2013) Software Defined Radio.

### 3.2.3. Data storage and access

The FRIPON stations are composed of a Linux minicomputer, a wide-angle camera and a manageable switch guaranteeing the isolation of the host institute's network. The installation is done with an automated deployment system based on a USB key.

When connecting to the host, the station establishes a secure VPN tunnel to the central server of the FRIPON project hosted by the IT department of the OSU Institut Pythéas (SIP) for all cameras and partner networks worldwide. The minicomputer is used for the acquisition and temporary storage of long exposure captures and detections through the FreeTure open source software (Audureau et al. 2014) and a set of scripts. The data, which include astrometric long exposures images, single detection (stacked images), multiple detections (both optical and radio raw data) are subsequently transferred to the central server.

The data collected on the server are then indexed in a database. During this operation, visuals are generated. When an optical event groups at least two stations, the FRIPON pipeline is executed to generate the dynamical and physical properties of the incoming meteoroid such as its orbit, its mass and its impact zone.

All the data is made available through a web interface that is accessible to the worldwide community in real time[3]. This interface makes it possible to display and download data in the form of an archive that complies with the project's data policy by means of access rights management.

### 3.2.4. Detection strategy

The acquisition and detection software FreeTure has been specifically developed by the FRIPON team and runs permanently on the minicomputers (see Audureau et al. 2014 for a full description). The images corresponding to single detections by FreeTure are stored locally and a warning (time and location) is sent to the central server in Marseille. If at least one other station detects an event within +/- 3 second, it is then treated as a "multiple detection". Note that we have implemented a distance criterion of less than 190 km to avoid false detections. This strategy works well at night time but leads to 30% of false detections mainly during twilight.

Radio data corresponding to the last week of acquisition are only stored locally. Only radio data acquired at the time of an optical multi-detection are uploaded from the radio stations to the Marseille data center for processing.

---

[3] https://fireball.fripon.org

### 3.3. Data processing

#### 3.3.1. Optical data

Scientific optical data are CCD observations recorded at a rate of 30 frames per second (fps). This acquisition rate is necessary to avoid excessive elongation of the meteor in the images in the case of high speed fireballs. For example, a bolide with an average speed of $20°/s$ leads to a four pixels elongated trail which is larger than the average width of the PSF (typically 1.8 pixels) but still easy to process for centroid determination. No dark and flatfield corrections are made.

However, almost no reference star is measurable on a single frame with such an acquisition speed as the limiting magnitude is about zero. It is thus necessary to record images with a longer exposure time for calibration. We therefore record five second exposure images every ten minutes, the goal being 1) to have a decent SNR up to a magnitude of 4.5 and 2) to only marginally affect detection efficiency. Such a calibration strategy allows the detection of a few thousand calibration stars for a given camera on a clear night. To mitigate the effect of cloudy nights and to get regular astrometric solutions, we compute an astrometric calibration every month for each station. The calibration procedure uses the ICRF2 reference frame. The distortion function of the optical system is computed in the topocentric horizontal reference system. This allows an astrometric solution for stars above 10 degrees of elevation with an accuracy of 1 arcminute. Our procedure leads to the calculation of the azimuth and the elevation of the bolides in the J2000 reference frame. More details regarding our astrometric calibration procedure can be found in Jeanne et al. (2019).

For the photometric reduction, we use the same frames as for the astrometric calibration, namely the long exposure ones. We then establish a correspondence between the observed stars and those present in the Hipparcos catalogue (Bessell 2000). The following steps are subsequently applied to calculate the absolute magnitude light curve of a meteor, namely: i) determination of the flux of an equivalent magnitude 0 star at zenith and of the linear extinction function of the air mass for one month cumulative observation; ii) measurement of the bolide flux on individual frames and conversion in magnitude iii) conversion of the meteor magnitude $Mag$ into an absolute magnitude $AMag$, defined as its magnitude at a distance of $100km$:

$$AMag_{fireball} = Mag_{fireball} - 5 \cdot \log_{10}\left(\frac{d}{100\text{km}}\right) \qquad (1)$$

Fig. 5 shows the final absolute magnitude lightcurve of an event recorded by 15 stations on February 27, 2019. We notice that the closest station (red curve) saturates faster with a -8 magnitude plateau compared to the other cameras.

Fig. 5 shows fireball lightcurves acquired by several stations. These lightcurves are saturated at different times depending on their distance to the bright flight. For the brightest part of the light curve, a saturation model will be applied in the future. Several limitations of our data reduction procedure need to be pointed out here:

– clouds may partly cover the night sky which may bias the measure of instrumental magnitudes;
– meteors are mainly detected at small elevations (typically below $30°/s$). These records are therefore affected by nonlinearities of the atmospheric extinction;
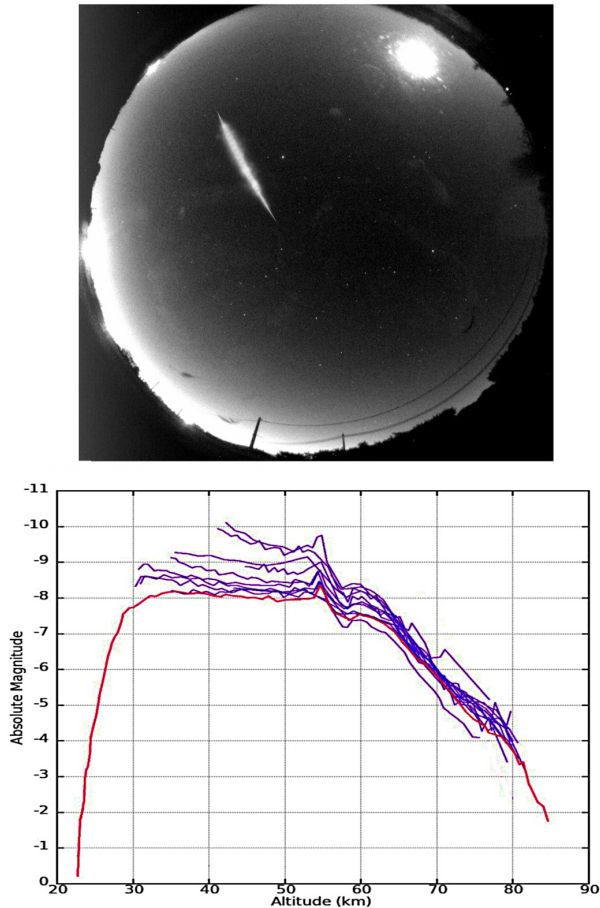
**Fig. 5.** Top: February 27, 2019 event seen by Beaumont-lès-Valence FRIPON camera;
Bottom: absolute magnitude light curves of the event as seen by 15 cameras, red curve is Beaumont-lès-Valence. It is clear that the saturation limit is around magnitude -8 (all the other light curves fall above this limit). Cameras located further away may be able to measure more non saturated data, but all the cameras do become heavily saturated as the bolide reaches its maximum luminosity.

– a uniform cloud layer can be the source of an under estimation of bolide magnitude.

To summarize, the astrometric reduction allows us to obtain an accuracy of 1/10 pixel or 1 arcmin for the meteor measurement. Photometry is at that time only usable for events with an absolute magnitude lower than $-8$ with an accuracy of 0.5 magnitude.

### 3.3.2. Trajectory determination

Most of our method is described in Jeanne et al. (2019) and in Jeanne (2020) and it will only be recalled briefly here.

Due to the limited accuracy of the Network Time Protocol (NTP, typically 20 ms, Barry et al. 2015), we assume that the trajectory follows a straight line, following the approach of Ceplecha (1987). This method allows us to separate the space and time components of our measurements and to overcome the problem of temporal accuracy. We give special attention to global error estimation, which becomes accessible thanks to the large number of cameras involved in most of FRIPON's detections. By comparison, the detections of other networks usually

involve fewer cameras, making external biases non measurable and hard to evaluate.

The density of the FRIPON network makes it possible to observe an event with many cameras (15 in the case of February 27, 2019 - see Fig. 5). It is then possible to consider the external astrometric bias of each camera as a random error and to estimate it by a statistical method. Therefore, we developed a modified least squares regression to fit the data taking into account the internal and the external or systematic error on each camera.

We first estimate the internal error of each camera by fitting a plane passing through the observation station and all the measured points. The average internal error of the cameras amounts to 0.75 arcmin, which corresponds to 0.07 pixel. We also compute a first estimation of the external error by averaging distance between the observed position of stars and those calculated from the Hipparcos catalogue (Bessell 2000) in a neighbourhood of 100 pixels around the meteor. We then compute a global solution using the modified least square estimator of the trajectory $\widehat{\mathcal{T}_{\chi^2}}$ given by the minimization of the following sum:

$$S(\mathcal{T}) = \sum_{i=1}^{n_{cam}} \sum_{j=1}^{n_i} \frac{\epsilon_{ij}(\mathcal{T})^2}{\sigma_i^2 + n_i s_i^2} \tag{2}$$

where $\epsilon_{ij}(\mathcal{T})$ is the residual between the $j^{th}$-measure taken by the $i^{th}$-camera and the trajectory $\mathcal{T}$, $\sigma_i$ is the internal error of the $i^{th}$-camera, $s_i$ is the systematic error of the $i^{th}$-camera, and $n_i$ is the number of images taken by the $i^{th}$-camera.

This method allows us to characterize the systematic errors of our cameras (e.g., a misaligned lens), but not errors such as the location of the camera. To tackle these errors, we compute a first estimate of the trajectory and we compare the residuals with the expected random and systematic errors. If they are larger than expected for a specific camera, we iteratively decrease its weight during the calculation of the trajectory. The final systematic error is usually of the order of 0.3 arcmin which ends the iterative process.

Two geometric configurations lead to important errors/degeneracies in the trajectory determination: (a) stations located too far from the fireball, and (b) stations aligned with the trajectory of the fireball. However, most of the time, the final bright flight straight line trajectory is known with a precision of a few tens of meters. In a second step, all individual data points are projected on the straight line.

### 3.3.3. Orbit, drag, and ablation model

To compute the orbit of a bolide, we need to measure its velocity before it has experienced significant interaction with the Earth-Moon system (hereafter infinite velocity). This interaction starts well before the bright flight. Therefore, we need a deceleration model to estimate the infinite velocity. This problem is complex because physical parameters evolve during atmospheric entry and moreover several parameters are unknown (drag coefficient, object size, shape, density, strength, etc...). Like other teams (Lyytinen & Gritsevich 2016; Sansom et al. 2019, etc...) we use a simple physical model to fit the bright flight data.

We use a dynamic model from Bronshten (1983), equations (3) and (4). This model describes the deceleration and the ablation of a meteoroid in an atmosphere based on the following three equations :

$$\frac{\mathrm{d}V}{\mathrm{d}t} = -\frac{1}{2}\rho_{atm}V^2c_d\frac{S_e}{M_e}\frac{s}{m} \qquad (3)$$

$$\frac{\mathrm{d}m}{\mathrm{d}t} = -\frac{1}{2}\rho_{atm}V^3c_h\frac{S_e}{HM_e}s \qquad (4)$$

$$s = m^\mu \qquad (5)$$

where $c_d$ is the drag coefficient, $c_h$ the heat-transfer coefficient, $H$ is the enthalpy of destruction, $\rho_{atm}$ is the gaz density, $m$ is the normalized meteoroid mass, $M_e$ is the pre-entry mass, $s$ is the normalized cross section area, $S_e$ is the pre-entry cross section area, $\mu$ is the so-called "shape change coefficient". The atmospheric gas density $\rho_{atm}$ is taken from the empirical model *NRLMSISE-00* (Lyytinen & Gritsevich 2016).

These three equations can be rewritten into two independent equations (Turchak & Gritsevich 2014). The equation of motion:

$$\frac{\mathrm{d}V}{\mathrm{d}t} = -\frac{1}{2}A\rho_{atm}V^2\exp\left(\frac{B}{A}\left(\frac{V_e^2}{2} - \frac{V^2}{2}\right)\right) \qquad (6)$$

and the equation of mass:

$$m = \exp\left(\frac{B}{A(1-\mu)}\left(\frac{V^2}{2} - \frac{V_e^2}{2}\right)\right) \qquad (7)$$

where $A$ is a deceleration parameter (in square meters per kilogram) and $B$ is an ablation parameter (in square meters per joule):

$$A = \frac{c_d S_e}{M_e} \qquad\qquad B = (1-\mu)\frac{c_h S_e}{HM_e}$$

With this model, the observation of a meteor motion makes it possible to estimate the value of the three parameters $V_e$, $A$, and $B$. Using $A$ and $B$ rather than their ratio $A/B$ (which is proportional to the enthalpy of destruction $H$ of the meteoroid; Turchak & Gritsevich 2014) allows us to avoid the numerical singularity when $B$ gets close to zero. Jeanne (2020) demonstrated that the least-squares estimators of these three parameters always have defined variances and meaningful values, even in the case of faint meteors. Finally, we compute confidence intervals in the three-dimensional parameter space ($V_e$, $A$, $B$).

### 3.3.4. Dark flight

At the end of the bright flight, a meteoroid is subject only to aerodynamic drag (including winds) and gravity. At this stage, the meteoroid speed is too low to cause ablation (hence dark flight).

The equation of motion during dark flight is as follows:

$$\frac{\mathrm{d}\vec{V}}{\mathrm{d}t} = \frac{1}{2}A_f(V_w)\rho_a V_w^2\vec{u_w} + \vec{g} \qquad (8)$$

where $A_f(V_w)$ is the deceleration parameter of the fragment which depends on the wind velocity (relative to the fragment) $V_w$. We use a local atmospheric model of wind retrieved from meteorological offices.

The end of the bright flight simulation gives us the initial conditions of the dark flight motion, namely the initial position, speed, and acceleration of the fragment. The initial condition of

acceleration give us a definition of $A_{f_0}$, the limit of $A_f$ when wind velocity is huge in front of sound velocity $c_s$:

$$A_{f_0} = A_f(V_w \gg c_s) = A\exp\left(\frac{V_0^2}{2}\cdot\frac{B}{A}\right) \qquad (9)$$

The evolution of $A_f$ as a function of wind velocity can be retrieved in Ceplecha (1987). Finally, we perform several computations using the Monte Carlo method to take into account the measurement errors of all the initial parameters in order to obtain a ground map (strewn field) as a function of the final mass of the bolide.

Of course, due to the various simplifying assumptions made, we can only underestimate the size of the strewn field. However, we can see that varying unknowns such as the object density or the drag parameter only cause the strewn field to slide along its center line. In the end, the main unknown is the width of that strewn field in the direction perpendicular to its center line that can be several hundred meters up to $1km$.

Taking the example of the January $1^{st}$, 2020 fall in Italy (Gardiol 2020), our determined strewn field with a 99% confidence level consisted of a thin strip 5.6 km long and 100 meters wide. The actual meteorite was found only 200 meters from the central line of this strip. This demonstrates the accuracy of our method, the small offset being mainly due to our ignorance of the actual meteorite shape.

## 4. First results

### 4.1. Statistics and network efficiency

One of the main objectives of the FRIPON network is to measure the unbiased incoming flux of extraterrestrial matter. In this section, we first present the raw statistics of detected falls. Next, we attempt to constrain the absolute flux of incoming material.

### 4.1.1. Raw meteoroid detections

Fig. 6 shows the histogram of duration and length of detected events. The average length of a meteor amounts to about $35km$ and it lasts for about 0.8s. Fig. 7 shows the detection rate of the network between January 2016 and March 2020 as well as the average number of monthly clear night sky hours. Between 2016 and January 2019, we observe an increase in the number of detections that reflects the increasing number of installed cameras. Since January 2019, the annual number of detections appears to be fairly constant at around 1,000 detections per year. Notably, the Perseid shower is the only shower standing out with regularity because of its high zenithal hourly rate (ZHR) and its long duration. The shorter Geminid shower is less prominent (e.g., 2017 and 2018) due to greater cloud coverage. Weak meteor showers are not unambiguously detected in our data due to the photometric detection limitation of our cameras. As expected, our study shows a strong correlation between the monthly detection rate and the percentage of clear sky due to the local climate and/or to seasonal variations (see Fig. 7 and Fig. 8).

Fig. 9 shows the radiants of $3,200$ fireballs detected since 2016 and Table 2 gives the number of detections for each shower per year. It shows that the main showers are detected and that
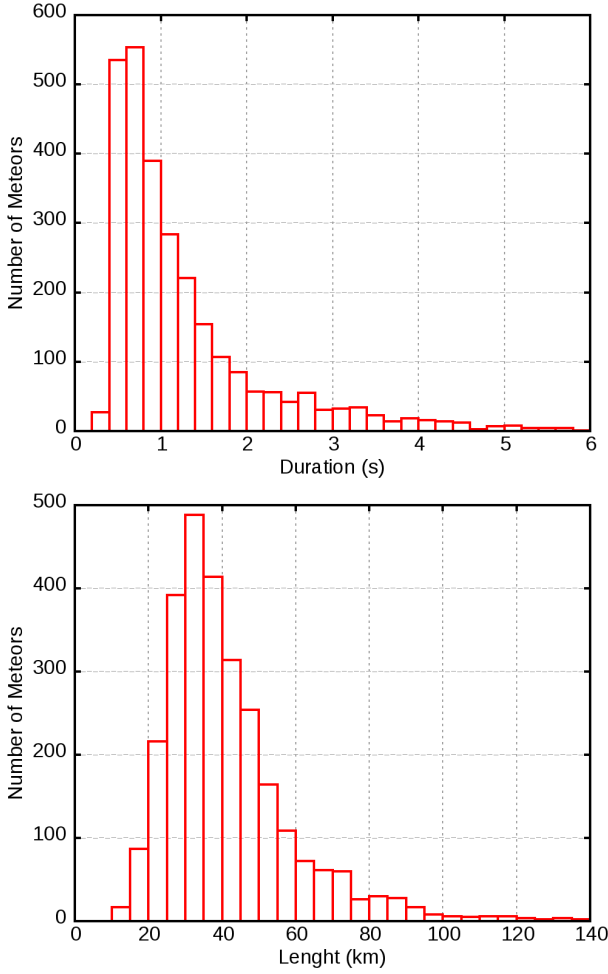
**Fig. 6.** Top: histogram of bright flight duration in seconds. Bottom : histogram of bright flight length in km. The 0.5s cut-off is due to the acquisition software FreeTure (Audureau et al. 2014).

the sporadic meteors are uniformly distributed over the celestial sphere except for part of the Southern hemisphere which is not at present within the reach of FRIPON. Overall, sporadic meteors represent 55% of the data.

### 4.1.2. Quantifying the absolute meteoroid flux

An important goal of the FRIPON network is to estimate the absolute flux of incoming meteoroids. For this purpose, it is mandatory to measure the efficiency of the network in terms of meteoroid discovery.

To estimate that flux, we need an estimation of the cloud coverage, of the percentage of stations down and of the sensitivity of our network as a function of meteor brightness. Regarding that last point, Fig. 10 shows the absolute magnitude histogram after three years of observations. Assuming a power law size distribution for interplanetary matter (Brown et al. 2002), it appears that FRIPON is clearly not fully efficient for events fainter than -4.5 in magnitude. This detection threshold is similar to that of the Prairie network (Halliday et al. 1996) and implies, as for other networks (Devillepoix et al. 2020), a minimum detection size of ~1 cm for incoming meteoroids. Note that smaller objects can nevertheless be detected if their entry speed is high enough.

To calculate the efficiency of FRIPON, we used only the French stations as these were the first to be installed and France

**Table 2.** Number of meteors observed for the different meteor showers per year. The empty columns correspond to showers that fall outside the observation period from December 2016 to December 2019. The Quadrantides (QUA) were not observed in 2018 due to a power outage during the first half of January.

| Code | total | 2016 | 2017 | 2018 | 2019 |
|------|-------|------|------|------|------|
| GEM | 329 | 86 | 42 | 82 | 119 |
| PER | 462 | – | 134 | 174 | 154 |
| CAP | 38 | – | 4 | 19 | 15 |
| QUA | 37 | – | 9 | – | 28 |
| LYR | 27 | – | 13 | 8 | 6 |
| LEO | 29 | – | 12 | 16 | 1 |
| SDA | 37 | – | 9 | 20 | 8 |
| ORI | 15 | – | 8 | 7 | 0 |
| NTA | 33 | 2 | 11 | 11 | 9 |
| MON | 11 | 3 | 2 | 4 | 2 |
| SPE | 11 | – | 3 | 5 | 3 |
| STA | 9 | – | 1 | 6 | 2 |
| ETA | 5 | – | 1 | 2 | 3 |
| HYD | 24 | 6 | 1 | 8 | 9 |
| EVI | 12 | – | 7 | 4 | 1 |
| JXA | 5 | – | 2 | 3 | 0 |

was fully covered in 2017. We considered its area, with a 120 km band added around it (Fig. 8) for a total of $10^6$ $km^2$, which was the basis for the calculation. For ≥1 cm meteoroids (i.e. for magnitude < -5 fireballs), we obtained an average rate of 250 events / year / $10^6$ $km^2$. Last, to estimate the incoming meteoroid flux for ≥1 cm bodies, we needed to correct for dead time (day time: 0.5 and average cloud cover: 0.4). The dead time corrected meteoroid flux for ≥1 cm meteoroids is 1,250 / year / $10^6$ $km^2$, which is comparable to the 1,500 / year / $10^6$ $km^2$ value given by Halliday et al. (1996).

### 4.1.3. Orbit precision

A precise determination of the orbit requires the extraction of a realistic initial velocity for the object. This can only be achieved by taking into account its deceleration in the upper atmosphere before the bright flight. Therefore our model of drag and ablation depends on three parameters (see section 3.3.3): the initial velocity *V*, a drag coefficient *A* and an ablation coefficient *B*. Depending on the quality of the data (number of cameras, weather conditions, distance of the camera, etc..), these three parameters do not have the same influence on the trajectory and cannot be determined with the same accuracy. We classified the meteors in three categories:

1. Those whose deceleration is hardly noticeable ($\widehat{A_{\chi^2}}/\sigma_A < 2$), which represent 65% of all meteors.
2. Those for which the deceleration is perceptible but not the ablation ($\widehat{A_{\chi^2}}/\sigma_A > 2$ and $\widehat{B_{\chi^2}}/\sigma_B < 2$), which represent 21% of all meteors.
3. Those whose deceleration and ablation are both perceptible ($\widehat{A_{\chi^2}}/\sigma_A > 2$ and $\widehat{B_{\chi^2}}/\sigma_B > 2$); which represent 14% of all meteors

For dynamical studies, only the detections that fall in one of the last two categories (35% of all detections) can be used. The typical velocity accuracy is then 100 m/s, which is required both for the identification of meteorite source regions in the Solar System (Granvik & Brown 2018) and for the search for
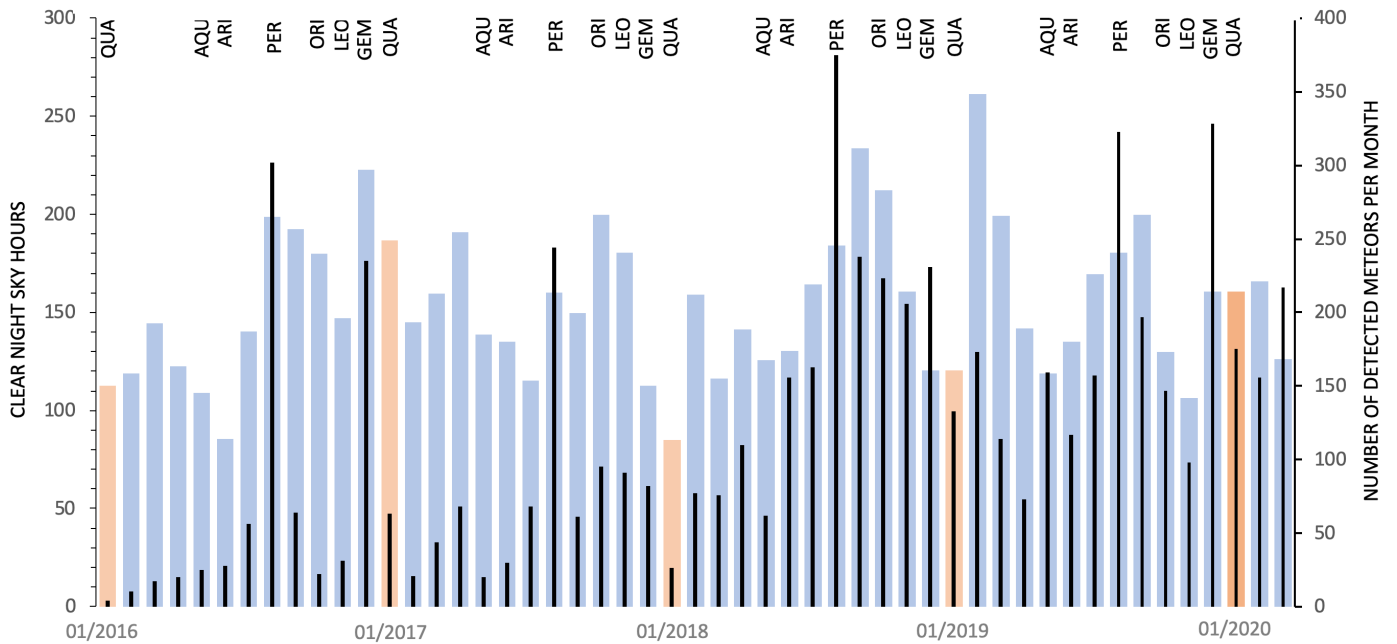
**Fig. 7.** Detection statistics for the last 3 years of operation. On a total of 3,700 trajectories computed: double 58%, triple 20%, quadruple 8%, and more than 4 simultaneous detections 14%. The number of detections (black bars) gradually increases as the installation of the stations progresses. Blue bars (orange for January) indicate the number of clear night sky hours each month, making it possible to also visualize the effect of cloud cover. The main meteor showers are listed at the top.
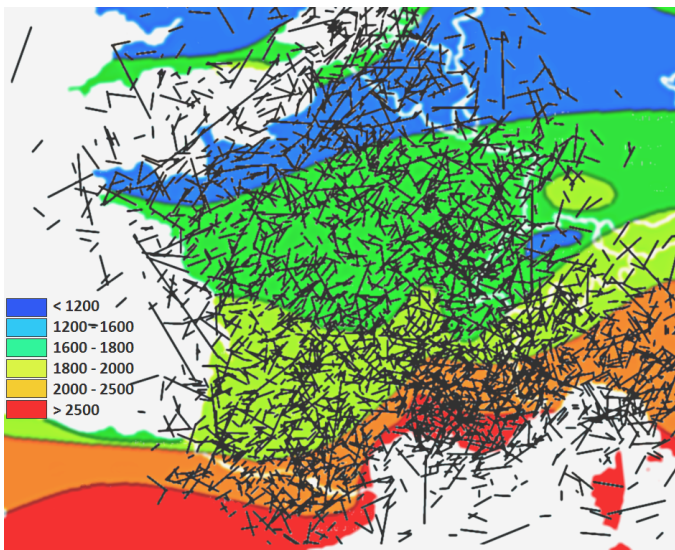


**Fig. 8.** Map of the 3700 trajectories measured with FRIPON data from 2016 to early 2020. The concentration of detections is in part explained by the background sunshine weather map (sunshine duration in hours per year). The Rhône valley and the South of France have twice as many clear nights as the North. Another factor is that the installation of the cameras, which was done mostly throughout 2016, started in Southern France and around Paris.

interstellar meteoroids Hajduková et al. (2019).

## 4.2. Dynamical properties of the observed meteoroids

In the following, we restrict our analysis to sporadic meteors. The histogram of initial velocities is shown in Fig. 11. It reveals two populations of meteoroids whose entry velocities differ by about $50 km/s$, suggesting an asteroidal (55%) and a cometary population (45%). This result can also be inferred from the histogram of meteoroid detections as a function of the inverse of the semi-major axis of their orbit (Fig. 12). This figure clearly shows a main belt population with semi-major axes between that of Mars and that of Jupiter, as well as a cometary population, possibly including Oort cloud material, with semi-major axes greater than that of Jupiter. Last, we do notice the presence of a few meteoroids with a negative semi-major axis. However, rather than concluding that interstellar matter was detected, we attribute these events to large errors associated with the calculation of their initial velocity. As a matter of fact, these events have semi-major axes that differ significantly from that of the interstellar object 1I/Oumuamua.

It is clear that in over 3 years of observation, FRIPON still has not detected any interstellar object. This compares to results obtained by other networks such as CMOR (Weryk & Brown 2004) who found only 0.0008 % of the objects detected that might be of interstellar origin. In the case of the FRIPON network, we can only give an upper limit of 0.1% but trust the real value to be much lower. Indeed, Hajduková et al. (2019) showed that no network so far has ever experienced a conclusive detection of an interstellar meteoroid. Most false detections are likely to stem from a bad error estimation, especially that of the initial speed, which requires an estimation of the drag coefficient.

## 4.3. Meteorite falls and first field search

Taking into account Halliday et al. (1989) and the surface area of the network, it should be possible to recover about ten meteorites per year weighting more than 100 g. Table 3 lists the events that produced a computed significant initial and/or final mass. The
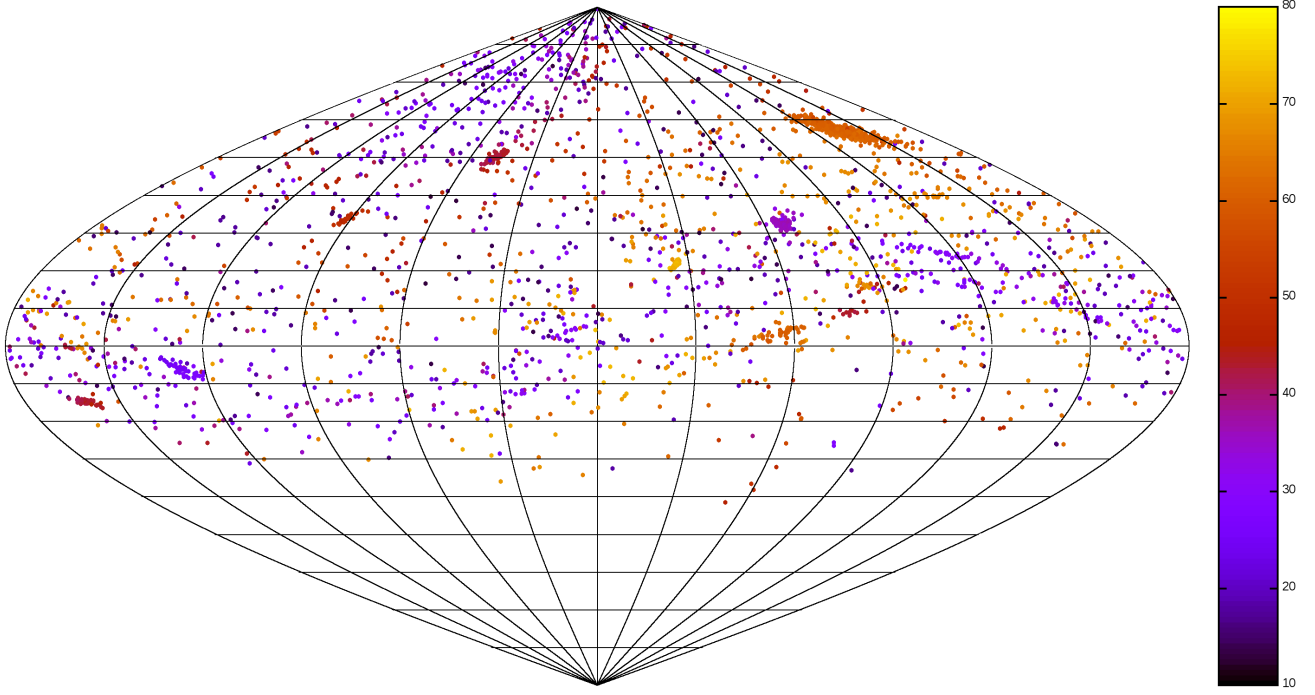
**Fig. 9.** Fireball radiant in Sanson-Flamsteed projection of equatorial coordinates from January 2016 to December 2019. The colour scale corresponds to the initial velocity of the objects: 1) low velocities (in blue) for asteroidal objects, 2) high velocities (in yellow) for cometary objects. The main showers are detected. 55% of the objects are sporadic: their radiants cover the sky uniformly except for its Southern part, which is invisible from European latitudes. The North toroidal sporadic source is visible in the upper left corner as well as low speed objects along the ecliptic plane coming from the anti-helion source.
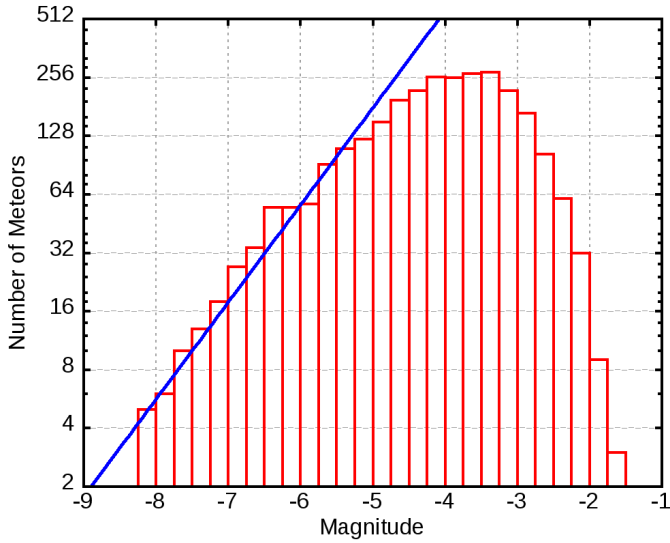


**Fig. 10.** Histogram of the absolute magnitude of the events detected by the network showing that the exhaustive detection regime is only reached around mag −5. The slope is compatible with that obtained by previous studies such as Brown et al. (2002), as shown on Fig. 13, which describes the distribution of interplanetary matter from from 1cm to 1km.
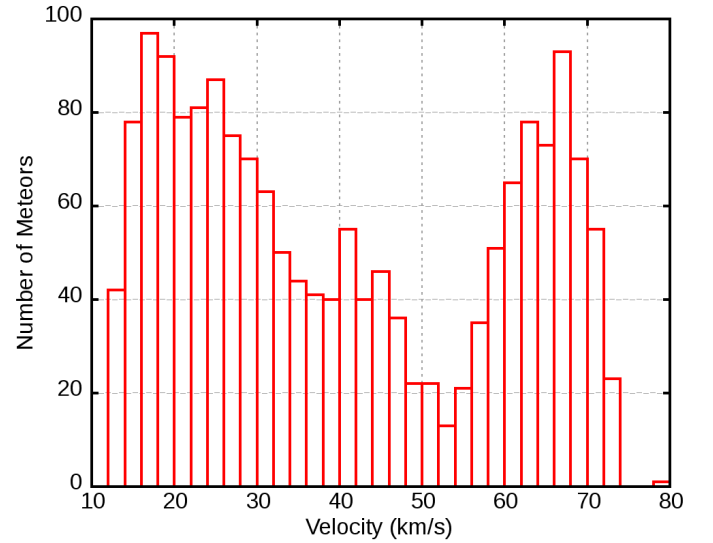
**Fig. 11.** Histogram of sporadic fireball entry velocities. Two populations can be observed: 1) low speed objects corresponding mostly to asteroidal orbits, 2) fast objects corresponding to TNOs or comet-like objects.

observed fall rate for final masses equal or greater than 100 g is 2.7 per year. This value is compatible with that of Halliday et al. (1996), once corrected to take into account the 20% overall efficiency of the FRIPON network (see above), which gives a corrected rate of 14 falls per year. Among these events, only one led to the recovery of meteorite fragments. This event occurred near Capodanno in Italy (Gardiol 2020) and was detected by the cam-

eras of the FRIPON-PRISMA network. Further details regarding the meteorite and its recovery will be presented in a forthcoming paper. This recovery is particularly important in showing that it is possible to find a 3 g stone thanks to the mobilization of the public with the help of various media (internet, newspapers...). This strategy has worked well and can be reproduced for all comparatively small falls (typically a few dozen grams). In such cases, it is clear the chances of finding the stone are low and do not
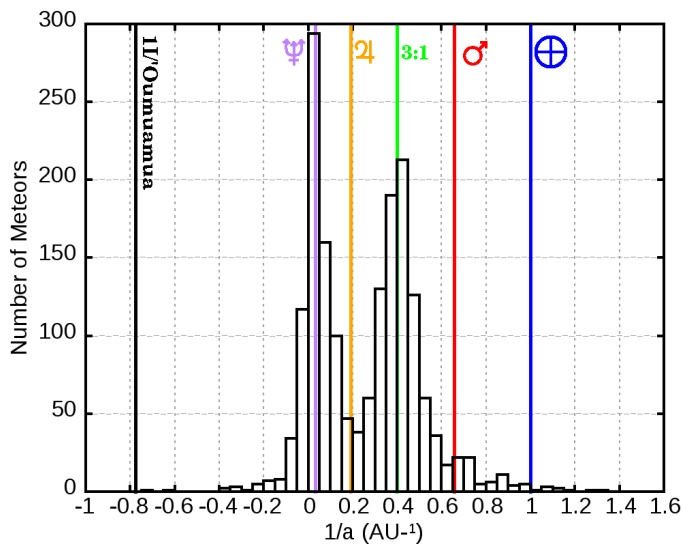
**Fig. 12.** Histogram of sporadic fireballs detected as a function of 1/a. This value is proportional to the orbital energy, making it possible to highlight two populations of objects: 1) the slow ones (of asteroidal origin) with a maximum related to the 3:1 and ν6 resonances (green line), which are the main sources of NEO; 2) the fast ones around Neptune (purple line). These two populations are separated by Jupiter (orange line). The figure also shows the orbits of the Earth (blue), of Mars (red) and of the interstellar object 1I/Oumuamua (black).

**Table 3.** 2016-2020 events with significant initial or final masses.

| Name | Date | Initial mass (kg) | Final mass (g) |
|---|---|---|---|
| Roanne | 2016 08 06 | 1.6 | 550 |
| Karlsruhe | 2016 09 25 | 5.3 | 0 |
| Carlit | 2016 11 27 | 3.0 | 200 |
| Chambord | 2017 03 27 | 1.0 | 60 |
| Rovigo | 2017 05 30 | 1.4 | 150 |
| Golfe du Lion | 2017 06 16 | 12.2 | 840 |
| Sarlat | 2017-08-04 | 1.4 | 110 |
| Avignon | 2017 09 08 | 1.8 | 5 |
| Luberon | 2017 10 30 | 2.7 | 17 |
| Menez-Hom | 2018 03 21 | 6.0 | 0 |
| Quercy | 2018 11 01 | 27.0 | 1 |
| Torino | 2018 12 27 | 1.6 | 550 |
| Sceautres | 2019 02 27 | 1.4 | 110 |
| Glénans | 2019 09 08 | 6.4 | 540 |
| Saar | 2019 10 13 | 1.3 | 270 |
| Bühl | 2019 10 16 | 1.2 | 0 |
| Capodanno | 2020 01 01 | 9.1 | 130 |
| Dole | 2020 02 16 | 1.5 | 950 |

warrant the organization of large searches, while an appeal to the general public may be fruitful. In the Capodanno case, the meteorite was found on a path by a walker and his dog.

It is also possible to calculate the meteorite flux for objects with final masses greater than 10g and compare it with previous estimates: Halliday et al. 1989 (81 /year / $10^6$ $km^2$), Bland et al. 1996 (225 /year / $10^6$ $km^2$) and Drouard et al. 2019 (222 /year / $10^6$ $km^2$). Given the limited accuracy of our mass estimate for light objects (about 100 % error), we chose start from the flux for objects with final masses greater than 100g, for which the accuracy is much higher. That flux is of 14 meteorite /year/$10^6$ $km^2$

(see above). We extrapolated it down to a mass of 10g, assuming a power law distribution of the final masses of the meteorites (Huss 1990), and obtained a value of 94 meteorites /year / $10^6$ $km^2$, close to the value from Halliday et al. (1989), also based on fireball data. It is, however, less than the other estimates (Bland et al. 1996 and Drouard et al. 2019), which are based on field searches.

## 5. Perspectives

### 5.1. Extension of the network

Significantly increasing the area covered by the network (by at least an order of magnitude) will be fundamental in increasing the recovery rate of meteorites, as this will lead to the detection, over a reasonable period, of a statistically significant number of very bright meteors that might be recovered on the ground as meteorites. Hence, there is a major interest in extending the FRIPON network over all of Europe and other parts of the world. Such an extension has already begun (see Fig. 1) and will be pursued over the coming years. The development plan includes, as a priority, the densification of the European coverage as well as its extension to southern countries such as Morocco, Algeria, and Tunisia. Such an extension would in itself would be sufficient to generate a network area about ten times larger that that of metropolitan France. In addition, the network is currently also being developed in Northern (Canada) and Southern (Chile) America. Fig. 13 shows that 30 objects larger than 1 meter fall on Earth ($510 \times 10^6 km^2$) every year. Taking into account the current surface area of the FRIPON network, the average expected detection rate of such objects is limited to an average of one in ten years. Extending the surface of the network is thus a necessity in order to reach an acceptable detection rate for 1 meter objects. Extending the network to EU and North Africa would make it reach a surface of $6 \times 10^6 km^2$, comparable to the Australian DFN network (Devillepoix et al. 2016), leading to a probability of a 1 meter event every $\sim$ 3 years.

### 5.2. Software

The reduction pipeline is operational and only requires minor improvements. The acquisition software FreeTure still shows a surprisingly high false detection rate, which requires that daylight observations are turned off at the moment. A new version using deep learning techniques is being developed so that daytime observations will become possible. The development of a tool to compute the lightcurve of heavily saturated events (Anghel et al. 2019b) is also planned.

### 5.3. Hardware

The hardware currently in use in the network corresponds to pre-2014 technology. A complete hardware update after 5 years of utilization is thus desirable to improve the temporal resolution of the ligthcurves as well as the performance and flexibility of the acquisition computers. A non exhaustive list of improvements includes upgrading from CCD to CMOS detectors and switching the current PCs to Raspberry Pi4 single board computers (SBCs).

In addition, a prototype of an all-sky radiometer is presently under development (Rault & Colas 2019), to resolve the saturation issue and improve on the bandwidth of the cameras. This
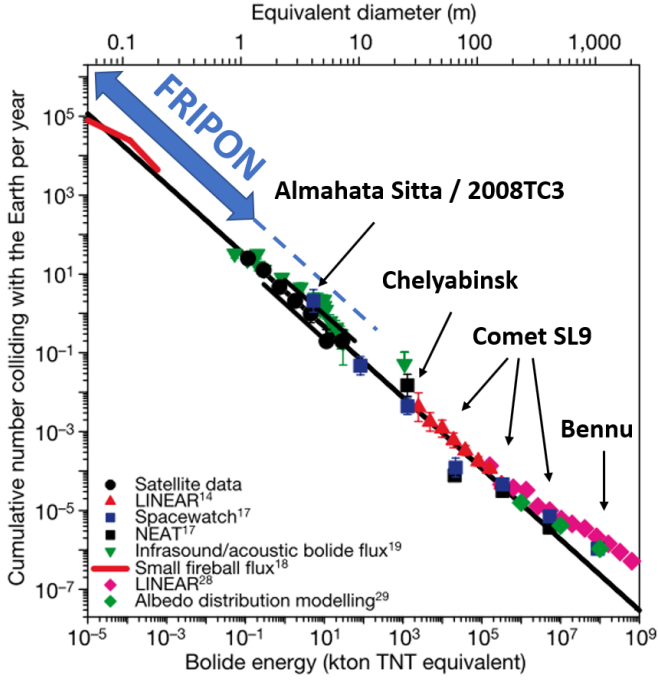
**Fig. 13.** Flux of small near-Earth objects colliding with the Earth (Brown et al. 2002). Data are shown over a range of 14 magnitudes in energy. The statistical model is based on near-Earth population for big sizes and, for the smaller ones, it is derived from a decade-long survey of ground-based observations of meteor and fireballs. FRIPON lies exactly between minor planets (detected by telescopes and planetary impacts) and interplanetary dust (detected by meteor networks). The solid arrow corresponds to FRIPON nominal mode, the dashed line is for rare events, observable by FRIPON but with too low a probability.

radiometer covers the visible and near infrared wavelengths. It is based on a 16 PIN photodiode matrix, followed by a trans-impedance amplification chain and a 14 bit industrial USB data acquisition module, which samples at a rate of 20 kHz. As an example, we superimposed on Fig. 14 the FRIPON camera lightcurve for an event of magnitude -9.5 which occured on August 14, 2019 at 03:07:02 UTC and the corresponding high data rate radiometer lightcurve.

### 5.4. Radio

The aim of FRIPON radio receivers is the accurate measurement of meteor velocities through the Doppler effect, allowing a much better determination of the orbital data (especially semi-major axes). In Table 4, we present the value of the initial velocity and effective surface-to-mass ratio derived for a meteor observed on October 15, 2018 at 1:15 UTC by 5 cameras. The accuracy achieved with the radio data leads to errors one order of magnitude lower compared to that achieved with the visible images only. However, it seems at present that only about 30 % of the optical detections lead to a detectable radio signal and that several bright radio events do not have any visible counterpart. For this reason, radio data have not been widely used yet, and further work is needed to improve our understanding of the complex phenomena associated with the generation of radio echoes by the plasma surrounding the meteors. Over time, we came to the conclusion that detailed information on the fragmentation and final destruction of bolides might also be obtained thanks to the head echoes produced by the GRAVES HPLA radar. Last, we detected unexpected oscillations (Rault et al. 2018) of the plasma envelope (see Fig. 15).
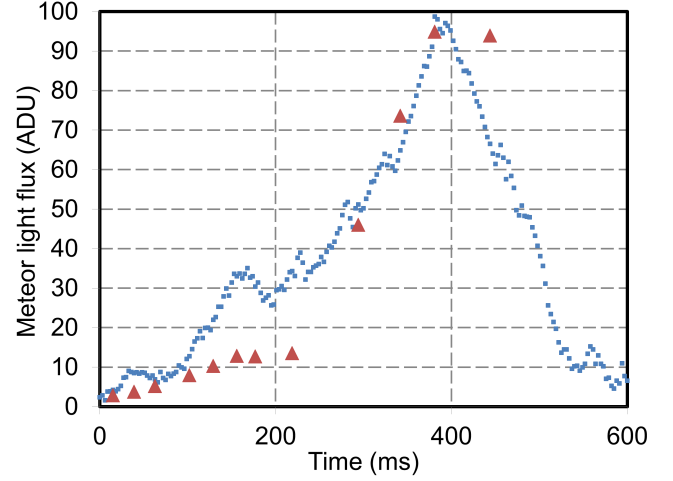


**Fig. 14.** Raw light flux from a bolide observed on August 14, 2019 at 03h07m02s UTC. Red triangles: Dijon FRIPON camera data (30 Hz, 12bits). Blue squares: radiometer prototype data (20 kHz, 14 bits). The faster acquisition rate and the higher amplitude dynamic range of the radiometer allows more detailed observations of the meteor fragmentation and of high speed luminosity variations.

**Table 4.** Velocity measurements on the bolide observed by 5 cameras on October 15, 2018 at 1h19m UTC.

| Sensor | Initial velocity $km/s$ | Effective surface / mass ratio $m^2/kg$ |
|--------|-------------------------|------------------------------------------|
| Video  | $66.49 \pm 0.92$        | $<1.28$                                  |
| Radio  | $66.09 \pm 0.09$        | $0.33 \pm 0.14$                          |
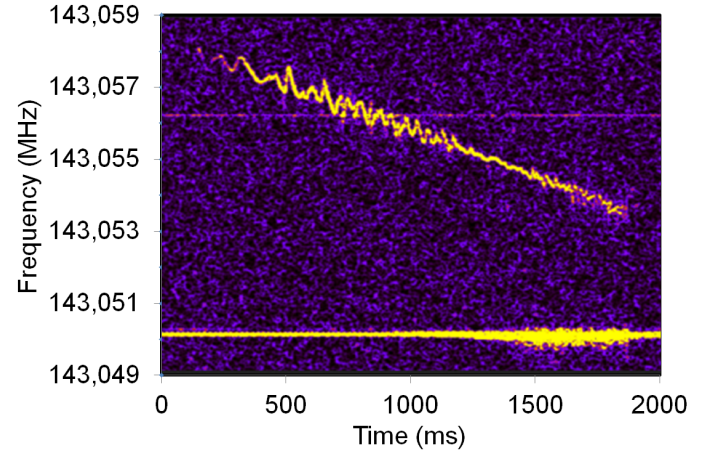


**Fig. 15.** Cyclic Doppler fluctuations on radio echo of the bolide observed on August 08, 2018 at 02h25m UTC, as seen by the Sutrieu radio receiver.

## 6. Conclusion

The FRIPON network, originally developed to cover the French territory, is now a fully automated camera network monitoring fireballs above part of Western Europe and a small fraction of Canada. As of today, it consists of 150 cameras covering an area

of about $1.5 \times 10^6\ km^2$. The level of automation of the network is such that a recovery campaign can be triggered only a few hours after a meteorite reached the surface of the Earth. We also developed an original orbit calculation algorithm with a precise and reliable error determination. It allows us to significantly enhance the statistics of orbital parameters of meteoroids, including those of interplanetary objects.

The FRIPON network has been monitoring meteoroid entries in Western Europe since 2016, allowing the characterization of the dynamical and physical properties of nearly 4,000 meteoroids. The distribution of their orbits appears bimodal, with a cometary population and a main belt one. Sporadic meteors amount to about 55% of all meteoroids. It thus appears that the range of sensitivity of the FRIPON network encompasses particles originating both from comets and from asteroids. A first estimate of the absolute flux of meteoroids bigger than 1cm amounts to 250 /year/$10^6\ km^2$, a value compatible with previous reports. We also estimate the flux of meteorites heavier than 100g to 14 /$10^6\ km^2$, a value compatible with data from other fireball networks but lower than those obtained from collecting meteorites. Finally, the first meteorite has been recovered in Italy based on the extended FRIPON network.

Further extension of the FRIPON network is under way. In the coming years, it will be extended to North Africa as well as Canada and South America. The goal is to reach a size large enough to allow the recovery of at least one fresh meteorite per year. In addition to the geographical extension of the network, technical developments will be conducted to improve the photometry of saturated images. Moreover, we plan to implement new algorithms in the detection software, so that daytime observations become possible and useful. Finally, we plan to fully exploit the radio network, both to improve current orbits and to reach a better understanding of the physical mechanism of meteoroid entries.

Last but not least, an extensive database of images that cover a large area may be used for additional purposes. The study of Transitory Luminous Events (TLE) such as sprites or spatial debris re-entries may be quoted as examples.

# References

Abbey, T. 2013, Journal of the British Astronomical Association, 123, 169

Anghel, S., Birlan, M., Nedelcu, D. A., & Boaca, I. 2019a, Romanian Astronomical Journal, 29, 189

Anghel, S., Birlan, M., Nedelcu, D.-A., & Boaca, I. 2019b, in EPSC-DPS Joint Meeting 2019, Vol. 2019, EPSC–DPS2019–1758

Audureau, Y., Marmo, C., Bouley, S., et al. 2014, in Proceedings of the International Meteor Conference, Giron, France, 18-21 September 2014, ed. J.-L. Rault & P. Roggemans, 39–41

Barghini, D., Gardiol, D., Carbognani, A., & Mancuso, S. 2019, A&A, 626, A105

Barry, M. A. T., Gault, D., Bolt, G., et al. 2015, PASA, 32, e014

Bessell, M. S. 2000, PASP, 112, 961

Bischoff, A., Barrat, J.-A., Bauer, K., et al. 2017, Meteoritics and Planetary Science, 52, 1683

Bischoff, A., Barrat, J.-A., Berndt, J., et al. 2019, Chemie der Erde / Geochemistry, 79, 125525

Bland, P. A., Smith, T. B., Jull, A. J. T., et al. 1996, MNRAS, 283, 551

Bland, P. A., Spurný, P., Bevan, A. W. R., et al. 2012, Australian Journal of Earth Sciences, 59, 177

Bland, P. A., Towner, M. C., Sansom, E. K., et al. 2016, in 79th Annual Meeting of the Meteoritical Society, Vol. 79, 6265

Borovicka, J., Spurný, P., Kalenda, P., & Tagliaferri, E. 2003, Meteoritics and Planetary Science, 38, 975

Borovička, J., Spurný, P., Brown, P., et al. 2013a, Nature, 503, 235

Borovička, J., Spurný, P., Šegon, D., et al. 2015, Meteoritics and Planetary Science, 50, 1244

Borovička, J., Tóth, J., Igaz, A., et al. 2013b, Meteoritics and Planetary Science, 48, 1757

Bradley, J. P., Keller, L. P., Brownlee, D. E., & Thomas, K. L. 1996, Meteoritics and Planetary Science, 31, 394

Bronshten, V. A. 1983, Physics of meteoric phenomena

Brown, P., Ceplecha, Z., Hawkes, R. L., et al. 1994, Nature, 367, 624

Brown, P., Hildebrand, A. R., Green, D. W. E., et al. 1996, Meteoritics and Planetary Science, 31, 502

Brown, P., McCausland, P. J. A., Fries, M., et al. 2011, Meteoritics and Planetary Science, 46, 339

Brown, P., Spalding, R. E., ReVelle, D. O., Tagliaferri, E., & Worden, S. P. 2002, Nature, 420, 294

Brown, P. G., Hildebrand, A. R., Zolensky, M. E., et al. 2000, Science, 290, 320

Brown, P. G., Vida, D., Moser, D. E., et al. 2019, Meteoritics and Planetary Science, 54, 2027

Ceplecha, Z. 1960, Bulletin of the Astronomical Institutes of Czechoslovakia, 11, 164

Ceplecha, Z. 1987, Bulletin of the Astronomical Institutes of Czechoslovakia, 38, 222

Chodas, P., Chesley, S., & Yeomans, D. 2010, in AAS/Division of Dynamical Astronomy Meeting #41, AAS/Division of Dynamical Astronomy Meeting, 6.03

Colas, F., Zanda, B., Bouley, S., et al. 2015, European Planetary Science Congress 2015, held 27 September - 2 October, 2015 in Nantes, France, id.EPSC2015-604, 10, EPSC2015

de la Fuente Marcos, C. & de la Fuente Marcos, R. 2018, Research Notes of the American Astronomical Society, 2, 57

Devillepoix, H. A. R., Bland, P. A., Towner, M. C., et al. 2016, in International Meteor Conference Egmond, the Netherlands, 2-5 June 2016, ed. A. Roggemans & P. Roggemans, 60–62

Devillepoix, H. A. R., Cupák, M., Bland, P. A., et al. 2020, arXiv e-prints, arXiv:2004.01069

Devillepoix, H. A. R., Sansom, E. K., Bland , P. A., et al. 2018, Meteoritics and Planetary Science, 53, 2212

Drouard, A., Gattacceca, J., Hutzler, A., et al. 2019, Geology, 47, 673

Duprat, J., Engrand, C., Maurette, M., et al. 2007, Advances in Space Research, 39, 605

Dyl, K. A., Benedix, G. K., Bland, P. A., et al. 2016, Meteoritics and Planetary Science, 51, 596

Fry, C., Melanson, D., Samson, C., et al. 2013, Meteoritics and Planetary Science, 48, 1060

Gardiol, D. 2020

Gardiol, D., Cellino, A., & Di Martino, M. 2016, in International Meteor Conference Egmond, the Netherlands, 2-5 June 2016, ed. A. Roggemans & P. Roggemans, 76

Granvik, M. & Brown, P. 2018, Icarus, 311, 271

Gritsevich, M., Lyytinen, E., Hankey, M., et al. 2017, in European Planetary Science Congress, EPSC2017–995

Haack, H., Michelsen, R., Stober, G., Keuer, D., & Singer, W. 2010, Meteoritics and Planetary Science Supplement, 73, 5085

Hajduková, Mária, J., Sterken, V., & Wiegert, P. 2019, Interstellar Meteoroids, ed. G. O. Ryabova, D. J. Asher, & M. J. Campbell-Brown, 235

Halliday, I., Blackwell, A. T., & Griffin, A. A. 1978, JRASC, 72, 15

Halliday, I., Blackwell, A. T., & Griffin, A. A. 1989, Meteoritics, 24, 173

Halliday, I., Griffin, A. A., & Blackwell, A. T. 1981, Meteoritics, 16, 153

Halliday, I., Griffin, A. A., & Blackwell, A. T. 1996, Meteoritics and Planetary Science, 31, 185

Huss, G. R. 1990, Meteoritics, 25, 41

Hutzler, A., Gattacceca, J., Rochette, P., et al. 2016, Meteoritics and Planetary Science, 51, 468

Jeanne, S. 2020, Méthode d analyse statistique appliquée au réseau dobservation européen des météores FRIPON - PhD thesis

Jeanne, S., Colas, F., Zanda, B., et al. 2019, A&A, 627, A78

Jenniskens, P., Fries, M. D., Yin, Q.-Z., et al. 2012, Science, 338, 1583

Jenniskens, P., Moskovitz, N., Garvie, L. A. J., et al. 2020, Meteoritics & Planetary Science, n/a [https://onlinelibrary.wiley.com/doi/pdf/10.1111/maps.13452]

Jenniskens, P., Rubin, A. E., Yin, Q.-Z., et al. 2014, Meteoritics and Planetary Science, 49, 1388

Jenniskens, P., Utas, J., Yin, Q.-Z., et al. 2019, Meteoritics and Planetary Science, 54, 699

Jones, J., Brown, P., Ellis, K. J., et al. 2005, Planet. Space Sci., 53, 413

Kokhirova, G. I., Babadzhanov, P. B., & Khamroev, U. K. 2015, Solar System Research, 49, 275

Kruijer, T. S. & Kleine, T. 2019, Geochim. Cosmochim. Acta, 262, 92

Lyytinen, E. & Gritsevich, M. 2016, Planet. Space Sci., 120, 35

McCrosky, R. E. & Boeschenstein, Jr., H. 1965, SAO Special Report, 173

McCrosky, R. E., Posen, A., Schwartz, G., & Shao, C.-Y. 1971, J. Geophys. Res., 76, 4090

Michal, T., Eglizeaud, J. P., & Bouchard, J. 2005, in ESA Special Publication, Vol. 587, 4th European Conference on Space Debris, ed. D. Danesy, 61

Nedelcu, D. A., Birlan, M., Turcu, V., et al. 2018, Romanian Astronomical Journal, 28, 57

Neveu, M. & Vernazza, P. 2019, ApJ, 875, 30

Oberst, J., Molau, S., Heinlein, D., et al. 1998, Meteoritics and Planetary Science, 33

Ott, T. & Drolshagen, e. 2020

Rault, J.-L., Birlan, M., Blanpain, C., et al. 2018, arXiv e-prints, arXiv:1804.05203

Rault, J.-L. & Colas, F. 2019, arXiv e-prints, arXiv:1911.04290

Rault, J.-L., Colas, F., & Vaubaillon, J. 2014, in Proceedings of the International Meteor Conference, Giron, France, 18-21 September 2014, ed. J.-L. Rault & P. Roggemans, 185–186

Rojas, J., Duprat, J., Engrand, C., et al. 2019, in Lunar and Planetary Science Conference, Lunar and Planetary Science Conference, 1968

Sansom, E. K., Jansen-Sturgeon, T., Rutten, M. G., et al. 2019, Icarus, 321, 388

Simon, S. B., Grossman, L., Clayton, R. N., et al. 2004, Meteoritics and Planetary Science, 39, 625

Spurný, P., Bland, P. A., Shrbený, L. ¡., et al. 2012, Meteoritics and Planetary Science, 47, 163

Spurný, P., Borovička, J., Baumgarten, G., et al. 2017, Planet. Space Sci., 143, 192

Spurný, P., Borovička, J., Kac, J., et al. 2010, Meteoritics and Planetary Science, 45, 1392

Spurný, P., Borovička, J. ., & Shrbený, L. ¡. 2020, Meteoritics and Planetary Science, 55, 376

Spurný, P., Haloda, J., Borovička, J., Shrbený, L., & Halodová, P. 2014, A&A, 570, A39

Spurný, P., Oberst, J., & Heinlein, D. 2003, Nature, 423, 151

Trigo-Rodríguez, J. M., Borovička, J., Spurný, P., et al. 2006, Meteoritics and Planetary Science, 41, 505

Trigo-Rodríguez, J. M., Llorca, J., Rubin, A. E., et al. 2009, Meteoritics and Planetary Science, 44, 211

Trigo-Rodríguez, J. M., Lyytinen, E., Gritsevich, M., et al. 2015, MNRAS, 449, 2119

Turchak, L. I. & Gritsevich, M. I. 2014, Journal of Theoretical and Applied Mechanics, 44, 15

Vernazza, P., Marsset, M., Beck, P., et al. 2015, ApJ, 806, 204

Weryk, R. J. & Brown, P. 2004, Earth Moon and Planets, 95, 221

Zolensky, M., Bland, P., Brown, P., & Halliday, I. 2006, Flux of Extraterrestrial Materials, ed. D. S. Lauretta & H. Y. McSween, 869–888

[1] IMCCE, Observatoire de Paris, PSL Research University, CNRS UMR 8028, Sorbonne Université, Université de Lille, 77 av. Denfert-Rochereau, 75014, Paris, France

[2] Institut de Minéralogie, Physique des Matériaux et Cosmochimie (IMPMC), Muséum National d'Histoire Naturelle, CNRS UMR 7590, Sorbonne Université, F-75005 Paris, France

[3] GEOPS-Géosciences Paris Sud, Université Paris-Sud, CNRS, Université Paris-Saclay, 91405, Orsay, France

[4] Aix Marseille Univ, CNRS, CNES, LAM, Marseille, France

[5] Aix Marseille Univ, CNRS, IRD, Coll France, INRA, CEREGE, Aix-enProvence, France

[6] Aix Marseille Université, CNRS, OSU Institut Pythéas UMR 3470 Marseille, France

[7] International Meteor Organization

[8] IAS, Université Paris Sud, Orsay, France

[9] FRIPON-Alsace, Vigie-Ciel Team

[10] FRIPON-Aquitaine, Vigie-Ciel Team

[11] FRIPON-Auvergne, Vigie-Ciel Team

[12] FRIPON-Bourgogne, Vigie-Ciel Team

[13] FRIPON-Bretagne, Vigie-Ciel Team

[14] FRIPON-Centre, Vigie-Ciel Team

[15] FRIPON-Champagne Ardennes, Vigie-Ciel Team

[16] FRIPON-Corse, Vigie-Ciel Team

[17] FRIPON-Franche-Comté, Vigie-Ciel Team

[18] FRIPON-Ile de France, Vigie-Ciel Team

[19] FRIPON-Languedoc-Roussillon, Vigie-Ciel Team

[20] FRIPON-Limousin, Vigie-Ciel Team

[21] FRIPON-Lorraine, Vigie-Ciel Team

[22] FRIPON-Midi-Pyrénées, Vigie-Ciel Team

[23] FRIPON-Nord-Pas-de-Calais, Vigie-Ciel Team

[24] FRIPON-Normandie, Vigie-Ciel Team

[25] FRIPON-Picardie, Vigie-Ciel Team

[26] FRIPON-Pays de la Loire, Vigie-Ciel Team

[27] FRIPON-Poitou-Charentes, Vigie-Ciel Team

[28] FRIPON-Provence-Alpes-Côte dAzur, Vigie-Ciel Team

[29] FRIPON-Rhône-Alpes, Vigie-Ciel Team

[30] INAF Osservatorio Astrofisico di Torino, Via Osservatorio 20, 10025 Pino Torinese, Italy

[31] FRIPON-Chile

[32] Natural History Museum, Burgring 7, A-1010 Vienna, Austria

[33] FRIPON-Belgium

[34] FRIPON-Spain

[35] FRIPON-Netherlands, European Space Agency, SCI-SC, Keplerlaan 1, 2201 AZ Noordwijk, NL

[36] PRISMA-Italy

[37] MOROI, Astronomical Institute of the Romanian Academy, Cuţitul de Argint 5, 040557 Bucharest, Romania

[38] Oukaimeden Observatory, High Energy Physics and Astrophysics Laboratory, Cadi Ayyad University, Marrakech, Morocco

[39] FRIPON-Brasil

[40] FRIPON-Germany

[41] FRIPON-Switzerland

[42] Vigie-Ciel Team

[43] Universciences, 30 avenue Corentin Cariou, 75019 Paris France

[44] REFORME, (http://www.reforme-meteor.net/)

[45] SCAMP-FRIPON, UK

[46] ESA/ESTEC, Noordwijk, The Netherlands

[47] Cosmos Sterrenwacht, Frensdorferweg 22, 7635 NK Lattrop, NL

[48] Cyclops Observatory, Duinbeekseweg 22, 4356 CE Oostkapelle, NL

[49] KVI - Center for Advanced Radiation Technology, Zernikelaan 25, 9747 AA Groningen, NL

[50] Leiden Observatory, Niels Bohrweg 2, 2333 CA Leiden, NL

[51] European Space Agency, OPS-SP, Keplerlaan 1, 2201 AZ Noordwijk,

[52] Università degli Studi di Torino Dipartimento di Fisica, Via Pietro Giuria 1, 10125 Torino, Italy

[53] Service Informatique Pythéas (SIP) CNRS - OSU Institut Pythéas - UMS 3470, Marseille

[54] Espace des Sciences, Planétarium, 10, Cours des Alliés Rennes France

[55] Université de Technologie de Compiègne, Rue Roger Couttolenc, 60200 Compiègne

[56] Vannes Astronomie, 14 Rue de la Tour d'Auvergne, 56000 Vannes

[57] Station de Radioastronomie de Nançay, Route de Souesmes, 18330 Nançay

[58] GISFI, Rue Nicolas Copernic, 54310 Homécourt

[59] Geosciences Environnement Toulouse, UMR5563 CNRS, IRD et Université de Toulouse, 14 avenue Edouard Belin,31400 Toulouse, France

[60] Villefagnan Observatory, Villefagnan, France

[61] Cerap Planétarium de Belfort, Cité des associations 90000 Belfort

[62] Club d'Astronomie du FLEP -"La rampisolle" 24660 Coulounieix-Chamiers - France

[63] Les Editions du Piat, Glavenas, 43200 Saint-Julien-du-Pinet - France

[64] Université Grenoble Alpes, CNRS, IPAG, 38400 Saint-Martin dHères France

[65] Institut Universitaire de France, Paris, France

[66] Geneva Observatory, CH-1290 Sauverny, Switzerland

[67] Institut de Paléoprimatologie, (iPHEP, UMR-CNRS 7262), UFR SFA,Université de Poitiers, 86022 Poitiers

[68] LPG-BIAF Faculté des sciences Géologie 49045 - Angers France
[69] FRIPON-Morroco
[70] Observatoire Astronomique de Valcourt, 52100 Valcourt France
[71] Planétarium LUDIVER, 1700, rue de la libération Tonneville 50460 La Hague
[72] Association Astronomique de Belle-Ile-en-mer 56360 Bangor, France
[73] Le Planétarium Roannais 42153 Riorges - France
[74] Bucharest University, Faculty of Physics, 405 Atomistilor, 077125 Magurele, Ilfov, Romania
[75] Groupe Astronomique de Querqueville, 50460 Cherbourg en Cotentin -France
[76] Laboratoire ICB, CNRS/Universite de Bourgogne, Dijon, France
[77] Société astronomique du Haut Rhin - 68570 Osenbach - France
[78] European Southern Observatory, Vitacura, Casilla 19001, Santiago de Chile, Chile
[79] Observatoire de Gramat, 46500 Gramat - France
[80] Carrefour des Sciences et des Arts, 46000 Cahors - France
[81] Observatoire de physique du globe de Clermont-Ferrand, 63170 Aubière - France
[82] INU champollion dphe, Place de verdun, 81000 Albi - France
[83] Observatório Nacional/MCTI, R. General José Cristino 77, Rio de Janeiro RJ 20921-400, Brazil
[84] Stella Mare - Universta di Corsica - CNRS 20620 Biguglia
[85] Association Astronomique "Les têtes en l'air" 79360 Marigny 79360
[86] Pôle des étoiles, Route de Souesmes, 18330 Nançay - France
[87] LPC2E, University of Orleans, CNRS, Orleans, France
[88] FRIPON - Peru
[89] CRPG - CNRS, 15 Rue Notre Dame des Pauvres, 54500 Vanduvre-lès-Nancy - France
[90] Observatoire de la Lèbe, Chemin des étoiles, 01260 Valromey-sur-Séran - France
[91] Armagh Observatory and Planetarium, Armagh BT61 9DG, Northern Ireland, UK
[92] Department of Geochemistry of Earth Sciences, Hassan II University, Casablanca, Morocco
[93] Shelyak Instruments, 77 Rue de Chartreuse, 38420 Le Versoud - France
[94] Parc du Cosmos, Avenue Charles de Gaulle 30133 Les Angles - France
[95] Eco musée de la baie du Mont Saint Michel, 50300 Vains Saint-Léonards - France
[96] Association Science en Aveyron, 12000 Rodez - France
[97] Aix-Marseille Université, PIIM UMR-CNRS, Marseille, France
[98] Observatoire de Narbonne, 11100 Narbonne
[99] Muséum des Volcans 15000 Aurillac - France
[100] Académie des sciences Institut de France - Château Observatoire Abbadia - 64700 Hendaye
[101] Brasserie Meteor, 6 Rue du Général Lebocq 67270 Hochfelden - France
[102] Astro-Centre Yonne, 77 bis rue émile tabarant Laroche 89400 St Cydroine - France
[103] Communauté de Communes du Canton d'Oust 5 chemin de Trésors, 09140 Seix France
[104] Société Astronomique de Touraine Le Ligoret 37130 Tauxigny
[105] Observatoire de Dax, Rue Pascal Lafitte 40100 Dax France
[106] Mairie, 4 Place de l'Église 36230 Saint Dens Les Jouhet - France
[107] Department of Physics and Astronomy, University of Western Ontario, London, Ontario, N6A 3K7, Canada
[108] Observatoire de La Perdrix, 25650 Hauterive-la-Fresse - France
[109] Université de Technologie de Troyes (UTT) 10004 Troyes - France
[110] Lycée Polyvalent d'Etat, route de l'Ospedale 20137 Porto-Vecchio
[111] Communauté de communes de Bassin d'Aubenas 07200 Ucel - France
[112] Service hydrographique et océanographique de la Marine, 29200 Brest - France
[113] laboratoire Morphodynamique Continentale et Côtière (M2C), UMR6143, Université de Caen, 14000 Caen
[114] FRIPON-Austria
[115] GEPI, Observatoire de Paris, Université PSL, CNRS, 77 Av. Denfert-Rochereau, 75014 Paris, France
[116] Pôle d'accueil universitaire Séolane, 04400 Barcelonnette - France
[117] Observatoire Populaire de Laval - Planétarium 53320 Laval - France
[118] Muséum national d'Histoire naturelle, 75005 Paris - France
[119] Institut de radioastronomie millimétrique, Université Grenoble Alpes 38400 Saint-Martin-d'Hères
[120] Laboratoire GSMA, UMR CNRS 7331, Université de Reims Champagne-Ardenne, 51687 Reims
[121] École dingénieurs en Sciences Industrielles et Numérique - Université de Reims Champagne-Ardenne 08000 Charleville-Mézières
[122] Lycée Robespierre, 62000 Arras
[123] Cité du Volcan, Bourg Murat 97418 Plaine des Cafres97421, Ile de La Réunion
[124] Observatoire des Makes, Les Makes, 97421 Saint-Louis Ile de la La Réunion
[125] Observatoire du Maido, OSU-Réunion, CNRS, 97460 Saint Paul, Ile de la Réunion
[126] FRIPON-Ile de la Réunion
[127] Observatoire du Pic des Fées - Le mont des oiseaux - 83400 Hyères
[128] Association AstroLab 48190 Le Bleymard - France
[129] E.P.S.A. Etablissement public des stations d'altitude 64570 La Pierre Saint Martin
[130] Observatoire de Boisricheux 28130 Pierres - France
[131] Association d'astronomie du pays Royannais: Les Céphéides 17200 Royan
[132] Observatoire de Rouen 76000 Rouen
[133] Communauté de Communes du Pays Châtillonnais 21400 Châtillon-sur-Seine
[134] Space sciences, Technologies Astrophysics Research (STAR) Institute, Université de Liège, Liège B-4000, Belgium
[135] IUT Chalon sur Saône, 71100 Chalon-sur-Saône
[136] Kepler-Sternwarte Planétarium, 71263 Weil der Stadt, Germany
[137] Royal Belgian Institute for Space Aeronomy, Brussels, Belgium
[138] Lycée Polyvalent Robert Garnier, 72405 La Ferté Bernard - France
[139] Observatoire des Pléiades, e des Pléiades, Beaumont lès Valence
[140] CEA, DAM, DIF, F-91297, Arpajon, France
[141] Uranoscope, Avenue Carnot 7, 77220 Gretz-Armainvilliers, France
[142] Observatoire de Haute Provence - CNRS - 04870 Saint-Michel-l'Observatoire, FRance
[143] High Enthalpy Flow Diagnostics Group, Institut für Raumfahrtsysteme, Universität Stuttgart, D70569 Stuttgart, Germany
[144] Club Ajaccien des Amateurs d'Astronomie, Centre de recherche scientifique Georges Peri 20000 Ajaccio
[145] Laboratoire de Planétologie et Géodynamique, UMR6112, CNRS, Université Nantes, Université Angers, Nantes, France
[146] Laboratoire dOcéanologie et de Géosciences UMR 8187, 62930 Wimereux France
[147] Blois Sologne Astronomie 41250 fontaines-en-sologne
[148] Planétarium dEpinal, 88000 Épinal
[149] Institut UTINAM UMR 6213, CNRS, Université Bourgogne Franche-Comté, OSU THETA, 25010 Besançon
[150] Arbeitskreis Meteore e.V, Germany

[151] La Ferme des Etoiles, 32380 Mauroux
[152] Bibracte, Mont Beuvray, 71990 Saint-Léger-sous-Beuvray
[153] Université de Montpellier, LUPM, Laboratoire Univers et Particules de Montpellier 34095 Montpellier
[154] Université du Maine, Département de Géosciences, 72085 Le Mans
[155] Récréa Sciences (CCSTI du LIMOUSIN) 23200 Aubusson
[156] Centro de Astronoma (CITEVA), Universidad de Antofagasta, 1270300 Antofagasta Chile
[157] Astronomical Institute of the Romanian Academy, Bucharest, RO-040557
[158] Division for Medical Radiation Physics and Space Environment, University of Oldenburg, Germany
[159] Observatoire du Jura, Chemin Des Ecoles 21, CH-2824 Vicques
[160] Le Don Saint 19380 Bonnet Elvert
[161] Mairie, Le Village, 66360 Mantet
[162] Planetarium de Bretagne, Route du Radome, 22560 Pleumeur Bodou

[163] Club St Quentin Astronomie, 02100 Saint Quentin

[164] MAYA (Moulins Avermes Yzeure Astronomie) 03000 Moulins

[165] Laboratoire de Géologie de Lyon : Terre, Planète, Environnement, UMR CNRS 5276 (CNRS, ENS, Université Lyon1) France

[166] IRAP, Université de Toulouse, CNRS, UPS, CNES, Toulouse, France

[167] Institut de Ciències del Cosmos (ICC-UB-IEEC), 1, Barcelona E-08028, Spain

[168] Parc Astronòmic Montsec, Ager E-25691, Spain

[169] Parc naturel régional des Landes de Gascogne, 33380 Belin-Béliet

[170] Laboratoire Lagrange, UMR 7293, CNRS, Observatoire de la Côte dAzur, Université de Nice Sophia-Antipolis, Nice, France

[171] Association Pierre de Lune, 16 rue Jean Parvy, 87600 Rochechouart

[172] Hotel De Ville, Plaine De Cavarc, 47330 Cavarc

[173] Planète et Minéral Association, 16 rue daussières 11200 Bizanet

[174] Marie, 85120 La Chapelle aux Lys

[175] Mairie, Place de l'Hôtel de ville, 39170 Saint-Lupicin

[176] Planétarium ET Centre de diffusion des Sciences, Le PLUS, 59180 Cappelle la Grande

[177] Université de Bordeaux, CNRS, LOMA, 33405 Talence

[178] Instituto de Astrofísica, PUC, Santiago, Chile

[179] Club Alpha Centauri, 11240 Cailhavel

[180] Lycée Pierre Forest, 59600 Maubeuge

[181] Mairie, 42300 Villerest

[182] Planétarium du Jardin des Sciences, 67000 Strasbourg

[183] Collège Robert Doisneau: association Sirius 57430 Sarralbe

[184] West University of Timisoara, Faculty of Mathematics and Computer Science, Romania

[185] Romanian Society for Cultural Astronomy

[186] Romanian Society for Meteors and Astronomy (SARM)

[187] Planétarium Rio Tinto Alcan / Espace pour la vie, Montréal, Québec, Canada

[188] Réseau DOME, (Détection et Observation de Météores / Detection and Observation of Meteors), Canada

[189] Department of Earth and Environmental Sciences, The University of Manchester

[190] UKMON, UK Meteor Observation Network

[191] School of Physical Sciences, The Open University

[192] European Space Agency, Oxford, UK

[193] Amgueddfa Cymru - National Museum Wales, Cardiff, Wales

[194] lycée Gustave Flaubert, La Marsa, Tunisia

[195] FRIPON - Tunisia

[196] Observatoire François-Xavier Bagnoud, 3961 St-Luc, Switzerland

[197] LFB - Lycée français de Barcelone - Bosch i Gimpera 6-10 - 08034 BARCELONA

[198] Grupo Ciencias Planetarias, Dep. Física Aplicada I Escuela de Ingeniería de Bilbao - Bilbao (Spain)

[199] Universidad del País Vasco/Euskal Herriko Unibertsitatea UPV/EHU Plaza Ingeniero Torres Quevedo 1, 48013 Bilbao

[200] Chair of Astronautics, TU Munich, Germany

[201] Herrmann-Lietz-Schule, Spiekeroog, Germany

[202] Förderkreis für Kultur, Geschichte und Natur im Sintfeld e. V., Fürstenberg, Germany

[203] EUC Syd, Sønderborg, Denmark

[204] Bundesanstalt für Geowissenschaften und Rohstoffe, Hannover, Germany

[205] Deutschen Schule Sonderburg, Denmark

e-mail: `Francois.colas@obspm.fr`

# Appendix A: Countries and observation stations involved in FRIPON

## Appendix A.1: Algeria

| Station | Long | Lat | Alt |
|---------|------|-----|-----|
| Alger | 3.033126E | 36.797014N | 342 |

## Appendix A.2: Austria

| Station | Long | Lat | Alt |
|---------|------|-----|-----|
| Wien | 16.359753E | 48.20525N | 180 |

## Appendix A.3: Belgium

| Station | Long | Lat | Alt |
|---------|------|-----|-----|
| Bruxelles | 4.357075E | 50.796727N | 114 |
| Liège | 5.566677E | 50.582574N | 240 |

## Appendix A.4: Brazil

| Station | Long | Lat | Alt |
|---------|------|-----|-----|
| Rio de Janeiro | 43.223311W | 22.8955612S | 50 |

## Appendix A.5: DOME - Canada

| Station | Long | Lat | Alt |
|---------|------|-----|-----|
| Louiseville | 72.949033W | 46.249248N | 30 |
| Montebello | 74.937772W | 45.660370N | 70 |
| Montréal | 73.550401W | 45.560745N | 30 |
| MontMegantic | 71.152584W | 45.455704N | 1110 |
| Val David | 74.207167W | 46.030661N | 327 |
| Val Saint François | 72.311258W | 45.493749N | 200 |

## Appendix A.6: Chile

| Station | Long | Lat | Alt |
|---------|------|-----|-----|
| Baquedano | 69.845453W | 23.335221S | 1500 |
| Chiu Chiu | 68.650429W | 22.342471S | 2525 |
| La Silla | 70.732559W | 29.260110S | 2400 |
| Peine | 68.068760W | 23.681256S | 2450 |
| San Pedro | 68.179340W | 22.953465S | 2408 |
| Cerro Tololo | 70.806279W | 30.169071S | 2207 |
| Cerro Paranal | 70.390400W | 24.615600S | 2518 |

## Appendix A.7: Denmark

| Station | Long | Lat | Alt |
|---------|------|-----|-----|
| Sonderborg | 9.798961E | 54.908907N | 190 |

## Appendix A.8: Vigie-Ciel - France

| Station | Long | Lat | Alt |
|---------|------|-----|-----|
| Aix en Provence | 5.333919E | 43.491334N | 184 |
| Ajaccio | 8.792768E | 41.878472N | 99 |
| Amiens | 2.298872E | 49.898572N | 39 |
| Angers | 0.600625W | 47.482477N | 58 |
| Angoulème | 0.164370E | 45.649047N | 100 |
| Arette | 0.741999W | 42.974571N | 1687 |
| Arras | 2.765306E | 50.287532N | 80 |
| Aubenas | 4.390887E | 44.621016N | 315 |
| Aubusson | 2.165551E | 45.955477N | 447 |
| Aurillac | 2.431090E | 44.924888N | 690 |
| Albi | 2.137611E | 43.918671N | 192 |
| Bangor | 3.186704W | 47.313333N | 57 |
| Barcelonette | 6.642280E | 44.389977N | 1162 |
| Beaumont les Valence | 4.923750E | 44.883366N | 174 |
| Belfort | 6.865081E | 47.640847N | 374 |
| Besançon | 5.989410E | 47.246910N | 311 |
| Biguglia | 9.479848E | 42.616786N | 8 |
| Bizanet | 2.873811E | 43.163547N | 85 |
| Brest | 4.504642W | 48.408671N | 66 |
| Caen | 0.366897W | 49.192307N | 58 |
| Cahors | 1.445918E | 44.455450N | 126 |
| Cailhavel | 2.125917E | 43.161526N | 254 |
| Cappelle la Grande | 2.366590E | 50.996056N | 12 |
| Caussols | 6.924434E | 43.751762N | 1279 |
| Cavarc | 0.644886E | 44.687615N | 113 |
| Chalon sur Saône | 4.857151E | 46.776202N | 186 |
| Chapelle aux Lys | 0.659221W | 46.628912N | 141 |
| Charleville | 4.720703E | 49.738458N | 187 |
| Chatillon sur Seine | 4.577100E | 47.864833N | 222 |
| Compiègnes | 2.801346E | 49.401338N | 48 |
| Coulounieix | 0.706613E | 45.154948N | 208 |
| Dax | 1.030458W | 43.693356N | 36 |
| Dijon | 5.073255E | 47.312718N | 285 |
| Epinal | 6.435744E | 48.185721N | 363 |
| Glux en Glenne | 4.029504E | 46.957773N | 688 |
| Gramat | 1.725729E | 44.745122N | 330 |
| Grenoble | 5.761051E | 45.192599N | 230 |
| Gretz-Armainvilliers | 2.742281E | 48.742632N | 112 |
| Guzet | 1.300228E | 42.787823N | 1526 |
| Hendaye | 1.749324W | 43.377440N | 87 |
| Hochfelden | 7.567531E | 48.756330N | 191 |
| Hyères | 6.112921E | 43.095433N | 240 |
| La Chatre | 1.866338E | 46.529210N | 28 |
| La Ferté Bernard | 0.647542E | 48.185502N | 95 |
| Laval | 0.782894W | 48.081912N | 103 |
| Le Bleymard | 3.737160E | 44.504370N | 1196 |
| Le Mans | 0.163854E | 48.015681N | 109 |
| Les Angles | 4.753658E | 43.961583N | 80 |
| Les Makes | 55.410097E | 21.198890S | 990 |
| Le Vaudoué | 2.522362E | 48.362668N | 80 |
| Le Versoud | 5.851000E | 45.211726N | 224 |
| Lille | 3.071544E | 50.614975N | 35 |
| Ludiver | 1.727798W | 49.630735N | 180 |
| Lyon | 4.866197E | 45.779935N | 190 |
| Maido | 55.383012E | 21.079594S | 2160 |
| Mantet | 2.306972E | 42.477420N | 1555 |
| Marigny | 0.417403W | 46.197592N | 59 |
| Marseille | 5.436376E | 43.343690N | 130 |
| Maubeuge | 3.987223E | 50.277947N | 145 |
| Mauroux | 0.819706E | 43.919035N | 225 |
| Migennes | 3.509820E | 47.968880N | 130 |

| Station | Long | Lat | Alt |
|---|---|---|---|
| Montpellier | 3.865524E | 43.632674N | 74 |
| Moulins | 3.319005E | 46.559871N | 217 |
| Nançay | 2.195688E | 47.367857N | 136 |
| Nantes | 1.554742W | 47.238106N | 26 |
| Onet le Chateau | 2.585813E | 44.364935N | 552 |
| Orléans | 1.943693E | 47.836332N | 120 |
| Orsay, GEOPS | 2.179331E | 48.706433N | 174 |
| Osenbach | 7.206581E | 47.992670N | 471 |
| Paris, MNHN | 2.357177E | 48.843075N | 55 |
| Paris, Observatoire | 2.336725E | 48.836550N | 88 |
| Pic de Bure | 10.335099E | 36.880495N | 2560 |
| Pic du Midi | 0.142626E | 42.936362N | 2877 |
| Pierres | 1.532769E | 48.579869N | 165 |
| Pleumeur Bodou | 3.527085W | 48.783253N | 35 |
| Poitiers | 0.380783E | 46.565784N | 130 |
| Pontarlier | 6.351011E | 46.914613N | 834 |
| Porto Vecchio | 9.271180E | 41.599753N | 22 |
| Puy de Dome | 2.964573E | 45.772129N | 1465 |
| Querqueville | 1.692611W | 49.665715N | 21 |
| Reims | 4.067164E | 49.243267N | 137 |
| Rennes | 1.674733W | 48.105705N | 100 |
| Roanne | 4.036814E | 45.996456N | 360 |
| Rochechouart | 0.819906E | 45.823100N | 250 |
| Rouen | 1.100422E | 49.447464N | 50 |
| Royan | 1.048922W | 45.639012N | 15 |
| Sabres | 0.746172W | 44.149087N | 85 |
| Saint Bonnet Elvert | 1.908838E | 45.165080N | 539 |
| Saint Denis de Jouhet | 1.866338E | 46.52921N | 280 |
| Saint Julien du Pinet | 4.054800E | 45.133304N | 961 |
| Saint Lupicin | 5.792866E | 46.397709N | 590 |
| Saint Michel (OHP) | 5.714722E | 43.933010N | 558 |
| Saint Quentin | 3.293955E | 49.862943N | 120 |
| Salon de Provence | 5.098180E | 43.642734N | 89 |
| Sarralbe | 7.021394E | 48.982666N | 229 |
| Strasbourg | 7.762862E | 48.579825N | 165 |
| Sutrieu | 5.626334E | 45.915575N | 867 |
| Talence | 0.59296W | 44.807851N | 48 |
| Tauxigny | 0.832971E | 47.223431N | 97 |
| Toulouse | 1.479209E | 43.562164N | 151 |
| Troye | 4.064624E | 48.270024N | 132 |
| Vains | 1.446219W | 48.663646N | 16 |
| Valcourt | 4.911772E | 48.616524N | 141 |
| VandoeuvreLesNancy | 6.155328E | 48.655893N | 373 |
| Vannes | 2.810623W | 47.503369N | 58 |
| Wimereux | 1.605850E | 50.762740N | 19 |

**Appendix A.9: Germany**

| Station | Long | Lat | Alt |
|---|---|---|---|
| Fürstenberg | 8.747344E | 51.516789N | 330 |
| Haidmühle | 13.758000E | 48.823000N | 820 |
| Hannover | 9.822995E | 52.405035N | 80 |
| Ketzur | 12.631277E | 52.495000N | 144 |
| Oldenburg | 8.165100E | 54.908907N | 123 |
| Seysdorf | 11.720225E | 48.545182N | 460 |
| Spiekeroog | 7.713935E | 53.773939N | 10 |
| Stuttgart | 9.103641E | 48.750942N | 300 |
| Weil der Stadt | 8.860460E | 48.751819N | 420 |

**Appendix A.10: PRISMA - Italia**

| Station | Long | Lat | Alt |
|---|---|---|---|
| Agordo | 12.031320E | 46.284320N | 600 |
| Alessandria | 12.031320E | 46.284320N | 107 |
| Arcetri | 11.254372E | 43.750590N | 100 |
| Asiago | 11.568190E | 45.849170N | 1365 |
| Barolo | 7.943960E | 44.611070N | 315 |
| Bedonia | 9.6324870E | 44.507693N | 550 |
| Brembate di Sopra | 9.582623E | 45.718831N | 295 |
| Camerino | 13.067126E | 43.146300N | 670 |
| Capua | 14.175158E | 41.121389N | 30 |
| Caserta | 14.332310E | 41.072620N | 14 |
| Castellana Grotte | 17.147777E | 40.875611N | 312 |
| Cecima | 9.078854E | 44.814460N | 670 |
| Cuneo | 7.540082E | 44.384776N | 559 |
| Felizzano | 8.437167E | 44.912736N | 122 |
| Finale Ligure | 8.327450E | 44.178270N | 35 |
| Genova | 8.936114E | 44.425473N | 310 |
| Gorga | 13.636000E | 41.392100N | 810 |
| Isnello | 14.021338E | 37.939684N | 580 |
| Lecce | 18.111235E | 40.335278N | 23 |
| lignan | 7.4783333E | 45.789861N | 1678 |
| Loiano | 11.331773E | 44.256571N | 787 |
| Luserna San Giovanni | 7.258267E | 44.827685N | 571 |
| Medicina | 11.644608E | 44.524383N | 35 |
| Merate | 9.4286111E | 45.705833N | 345 |
| Montelupo Fiorentino | 11.043198E | 43.755337N | 500 |
| Monteromano | 11.635978E | 44.138456N | 765 |
| Monte Sarchio | 14.645457E | 41.063718N | 298 |
| Napoli | 14.255361E | 40.862528N | 102 |
| Navacchio | 10.491633E | 43.683200N | 15 |
| padova | 11.868540E | 45.401945N | 64 |
| Palermo | 13.299417E | 38.187283N | 35 |
| Piacenza | 9.725030E | 45.035376N | 77 |
| Pino Torinese | 17.764939E | 45.041240N | 620 |
| Pontevaltellina | 9.981636E | 46.190379N | 1207 |
| Reggio Calabria | 15.660189E | 38.119310N | 100 |
| Roma | 12.485338E | 41.894802N | 52 |
| Rovigo | 11.795048E | 45.081666N | 15 |
| SanMarcello Pistoiese | 10.803850E | 44.064155N | 1000 |
| Sardinia Radio Telescope | 9.130760E | 39.281950N | 100 |
| Savignano | 12.392745E | 44.089660N | 100 |
| Scandiano | 10.657597E | 44.591002N | 153 |
| Serra la Nave | 14.978864E | 37.691831N | 1725 |
| Sormano | 9.2285806E | 45.883000N | 1131 |
| Trento | 11.140785E | 46.065509N | 500 |
| Tricase | 18.366199E | 39.923622N | 94 |
| Triestre | 13.875086E | 45.642691N | 412 |
| Vicenza | 11.534934E | 45.558383N | 39 |

**Appendix A.11: Mexico**

| Station | Long | Lat | Alt |
|---|---|---|---|
| San Pedro Martir | 115.465753W | 31.045931N | 2830 |
| Ensenada | 116.666651W | 31.869425N | 50 |

**Appendix A.12: Morocco**

| Station | Long | Lat | Alt |
|---|---|---|---|
| Casablanca | 7.634891W | 33.596191N | 15 |
| Oukaimeden | 7.866467W | 31.206160N | 2725 |
| Ben Guerir | 7.936012S | 32.218554N | 460 |

*Appendix A.13: Netherland*

| Station | Long | Lat | Alt |
|---|---|---|---|
| Denekamp | 6.965788E | 52.414965N | 27 |
| Dwingeloo | 6.234525E | 52.484699N | 16 |
| Groningen | 6.5256694E | 53.249458N | 21 |
| Noordwijk | 4.418402E | 52.218752N | 25 |
| Oostkapelle | 3.537670E | 51.571920N | 4 |

*Appendix A.14: MOROI - Romania*

| Station | Long | Lat | Alt |
|---|---|---|---|
| Barlad | 27.671676E | 46.230847N | 81 |
| Berthelot | 22.889832E | 45.614765N | 400 |
| Bocsa | 21.777756E | 45.384465N | 283 |
| Bucuresti | 26.096667E | 44.413333N | 81 |
| Dej | 21.230793E | 45.738060N | 101 |
| Feleac | 23.593715E | 46.710241N | 800 |
| Galati | 28.031919E | 45.419133N | 81 |
| Madarjac | 27.134554E | 47.045297N | 200 |
| Marisel | 23.075184E | 46.660976N | 1200 |
| Paulesti | 25.978060E | 45.006917N | 242 |
| Timisoara | 21.230793E | 45.738060N | 101 |

*Appendix A.15: SPMN - Spain*

| Station | Long | Lat | Alt |
|---|---|---|---|
| Barcelona | 2.119061E | 41.391765N | 97 |
| Bilbao | 2.948512W | 43.262257N | 60 |
| Montsec | 0.736836E | 42.024865N | 820 |

*Appendix A.16: Switzerland*

| Station | Long | Lat | Alt |
|---|---|---|---|
| Saint Luc | 7.612583E | 46.228347N | 2200 |
| Vicques | 7.420632E | 47.351819N | 600 |

*Appendix A.17: Tunisia*

| Station | Long | Lat | Alt |
|---|---|---|---|
| la marsa | 10.335108E | 36.880492N | 20 |
| Sousse | 10.611125E | 35.812668N | 15 |

*Appendix A.18: SCAMP - UK*

| Station | Long | Lat | Alt |
|---|---|---|---|
| Armagh | 6.649632W | 54.352350N | 75 |
| Canterbury | 1.072080E | 51.273500N | 21 |
| Cardiff | 3.177870W | 51.486110N | 33 |
| East Barnet | 0.169234W | 51.637359N | 87 |
| Harwell | 1.315363W | 51.572744N | 90 |
| Honiton | 3.184408W | 50.801832N | 170 |
| Manchester | 2.233606W | 53.474365N | 70 |